Comparison of different methods for the detection of mesoscale eddy characteristics in the eastern tropical North Atlantic

---

Bachelor Thesis

B. Sc. Physics of the Earth System:
Meteorology, Oceanography, Geophysics

Christian-Albrechts-Universität zu Kiel
GEOMAR Helmholtz Center for Ocean Research

Author: Alexandra Andrae

Matriculation Number: 1120284

First Examiner: Dr. Marcus Dengler

Second Examiner: Dr. Torge Martin

December 2020

I. Zusammenfassung

Mesoskalige Wirbel spielen in vielen Bereichen des Ozeans eine wichtige Rolle. Die meisten Methoden, um Wirbel zu identifizieren und ihre Eigenschaften zu bestimmen, basieren auf Satellitendaten der Meeresoberflächenauslenkung und ihrer Anomalien. Durch ihre globale Abdeckung sowie ihre tägliche Bereitstellung eignen sich Satellitendaten hervorragend zur Wirbelbestimmung und -verfolgung über große Distanzen und lange Zeiträume. Jüngste Studien zweifeln die Eignung von Satellitendaten zur Wirbelerkennung an und zeigen, dass die Qualität der erzeugten Karten nicht nur stark unter Interpolation leidet, sondern auch, dass die Rasterauflösung entscheidend für die Wirbelbestimmung ist. Um herauszufinden, wann es sich um eine gute Wirbelbestimmung handelt und wann die Wirbelparameter unter der Interpolation leiden, vergleicht diese Arbeit eine satellitenbasierte Methode namens Angular Momentum Eddy Detection and Tracking Algorithm (AMEDA) mit einem auf insitu-Geschwindigkeitsmessungen basierenden, nichtlinearen Dämpfungsalgorithmus zur Gauss-Newton Optimierung. Dabei werden verschiedene Schwellwerte definiert, die helfen sollen, falsche Wirbelidentifizierungen anhand von Satellitendaten zu erkennen. Insgesamt wurden sieben Wirbel verglichen, die mit beiden Methoden gefunden wurden. Dabei variierte der Radius aus den Schiffsmessungen zwischen 30 und 46 km, die maximalen azimutalen Geschwindigkeiten lagen zwischen 20 und 50 $^{cm}/_{s}$ mit Rossbyzahlen zwischen 0.13 und 0.33. Die satelliten-basierte Methode überschätzte die Radien im Mittel um 68%, während die azimutalen Geschwindigkeiten um 44% unterschätzt wurden. Es zeigte sich außerdem, dass bei großen Rossbyzahlen die Eigenschaften der Wirbel durch die Satelliten sehr genau bestimmt wurden, während Wirbel bei Rossbyzahlen kleiner als 0.04 meistens als Falschidentifizierungen erkannt wurden. Als weitere Möglichkeiten zur Beurteilung der Satellitendaten wurden die Meeresoberflächentemperatur und die Meeresoberflächenauslenkung entlang der ursprünglichen Satellitenbahnen analysiert. Es ergab sich, dass diese Daten ebenfalls helfen können, falsche Wirbelnäherungen zu identifizieren. Außerdem wurden weitere Schwellwerte zu minimaler Lebensdauer von Wirbeln (7 Tage), minimalem Radius (40 km) und minimaler azimutaler Geschwindigkeit (6 $^{cm}/_{s}$) definiert.

II. Abstract

Mesoscale eddies play an important role in the whole ocean system. Eddy detection is most commonly based on satellite products, more precisely on altimetry. With the global coverage and their availability on a daily basis satellite data offers a great opportunity for eddy detection and tracking. Nevertheless, recent studies showed that the quality of derived eddy characteristics highly depends on the grid resolution of satellite products and suffer from interpolation and smoothing. To be able to distinguish between good estimates and those which suffer from interpolation, this study compares satellite derived eddy characteristics by an Angular Momentum Eddy Detection and Tracking Algorithm (AMEDA) to a nonlinear, damping Gauss-Newton optimization algorithm which uses ship-measured current velocities in the eastern tropical North Atlantic. Therefore, this study defines thresholds to qualify satellite-based estimates. In total, 7 eddies were found by both methods with radii ranging between 30 and 46 km and a maximum azimuthal velocity ranging between 20 and 50 $^{cm}/_{s}$. The Rossby number was calculated and ranged between 0.13 to 0.33. AMEDA overestimated the radii by 68% and underestimated the azimuthal velocity by 44% on average. Accurate satellite-based estimates appeared for large values of the Rossby number while values smaller than 0.04 showed false detection. Sea surface temperature and along-track data of sea level anomaly were further investigated with the conclusion that both data sets can help validating the satellite-based estimates depending on the case. Other thresholds like a minimum lifetime of 7 days, a minimum radius of 40 km and a minimum azimuthal velocity of 6 $^{cm}/_{s}$ can be introduced to qualify satellite-based estimates.

III Table of Contents

1. Introduction

Mesoscale eddies are nonlinear coherent vortices in the ocean on a scale from 20-200km. Their lifespan varies from days to years. Due to their non-linearity, vortices have the ability to trap water inside their cores. With that trapped water, they can travel long distances and transport water properties such as heat or salt as well as nutrients or phytoplankton. Therefore, they play an important role in the global mixing processes as well as in the distribution of e.g. heat, mass or energy (e.g. Chelton et al., 2011b,a; Amores et al., 2018). In addition, they can influence marine systems, biogeochemical cycles, near surface winds and clouds or rainfall (Chaigneau et al., 2008; Marina, 2008). Improving our knowledge of mesoscale eddies and their characteristics will expand our understanding of the whole ocean system (Lachkar and Gruber, 2012; Frenger et al., 2013).

The eastern tropical North Atlantic (ETNA) is among the important eastern boundary upwelling systems. Coastal upwelling brings cold, fresh and nutrient-rich waters to the surface which causes a high biological productivity (e.g., Lachkar and Gruber, 2012). With their ability to trap water, eddies can transport this coastal water to the open ocean (e.g., Chaigneau et al., 2008). Schütte et al. (2016) investigated eddies in the ETNA and found about 146 eddies per year with a minimum lifetime of seven days and a mean radius of about 56 km. The propagation speed in westward direction was identified as about 3 $^{\mathrm{km}}/_{\mathrm{day}}$. The horizontal length scale of mesoscale eddies is largely compared to the first baroclinic mode Rossby radius of deformation R_d, which is defined as $R_d = \frac{c_1}{f}$ where c_1 is the phase speed of an internal gravity wave of the first baroclinic mode and f the Coriolis parameter. Since R_d depends on f, it varies with latitude. It is largest close to the equator and decreases polewards. In the ETNA region R_d reaches values about 40-60 km (Chelton et al., 1998).

To be able to study eddies and their role in the ocean system, one needs to detect them and identify their properties first. Over the last decades, various approaches have been introduced which identify and track eddies and their properties using satellite data. With satellite altimetry, one can measure the sea surface height (SSH) and derive sea level anomalies (SLA) which describes the difference of the SSH over a reference ellipsoid and the temporal mean of SSH over a reference period. Eddies depending on their sense of rotation - cyclonic (anticlockwise) or anticyclonic (clockwise) - either create a negative or a positive value of SLA, respectively (Chelton et al., 2011b).

Eddy detection methods can be roughly split into three categories: The earliest approaches only use geometrical parameters, such as the velocity field or altimetric sea surface maps, some later ideas use dynamical parameters and the latest methods manifested on hybrid

approaches combining both geometrical and dynamical parameters (Le Vu et al., 2018; Aroucha et al., 2020). The desire to track eddies and to identify their properties with automatic algorithms reaches back to the year 1950 when McWilliams (1990) was one of the first who used relative vorticity (Aroucha et al., 2020). This method was picked up by Doglioli et al. (2007), who optimized it by using a wavelet analysis of the vorticity field (Le Vu et al., 2018). Chelton et al. (2011b) stated that eddies are not the only contributors to the SLA field. Therefore, dynamical parameters were introduced, such as the Okubo-Weiß parameter (Okubo, 1970; Weiss, 1991). If applied to the dataset, it separates vorticity dominated regions from strain dominated regions (Isern-Fontanet et al., 2006; Schütte et al., 2016; Chelton et al., 2007; Chaigneau et al., 2008). In other words, it distinguishes rotation from deformation. Eddies are likely to be found in vorticity dominated regions. A disadvantage is, that the Okubo-Weiß method requires thresholds for minimum size and lifespan which may be difficult to determine for the global ocean (Chelton et al., 2011b). Other threshold-free studies make use of closed contour lines of SLA or closed streamlines surrounding a SLA extremum (Chelton et al., 2011b; Faghmous et al., 2015; Schütte et al., 2016).

Le Vu et al. (2018) introduced an automated hybrid method based on both geometrical and dynamical parameters. Their goal was to create a robust and most precise method with variable input possibilities and a minimum amount of user tunable parameters. The so called Angular Momentum Eddy Detection and Tracking Algorithm (AMEDA) provides various eddy properties such as centre position, velocity and radius. In addition, it is also able to track eddies over time and identify merging and splitting events.

But nevertheless, all mentioned methods are based on satellite products as for example maps of sea surface height or sea surface anomaly. Satellites provide data sets of the oceans surface properties with global coverage on a daily basis. Furthermore, they cover long time series since the first altimetry satellite was launched in 1978 and is therefore a useful tool for eddy detection and tracking. Gridded satellite data is limited by its resolution which depends on the satellite tracks and their re-visit time period. Smoothing and interpolating of the along-track data is necessary to create gridded data on a daily basis. Investigating the individual satellite tracks, one notices that they can be further apart than the Rossby radius of deformation (Amores et al., 2018). Therefore, eddies with small radii ($\sim$40 km) can not be represented in an adequate way (Chelton et al., 2011b). Consequently, it can lead to errors in calculating the altimetric derived eddy properties (Ioannou et al., 2017; Garreau et al., 2018). Amores et al. (2018) questioned the ability to detect and track eddies from gridded SLA maps. They applied a tracking algorithm from Faghmous et al. (2015) to different SLA products inter alia to the SLA product from

Copernicus Marine Environment Monitoring Service (CMEMS) with $1/4° \times 1/4°$ resolution which is used in this study as well as to an high resolution model $1/60° \times 1/60°$. They showed that only 6% of the real eddies in the North Atlantic were found by CMEMS and a synthetic satellite-like product derived from the model. In addition, it was concluded that the horizontal length scale of eddies is highly overestimated and that smaller eddies (R<40 km) can not be captured by satellite-like products. Moreover, several small eddies are likely to be merged to a larger one (Amores et al., 2018). They also pointed out that the smoothing, gridding and interpolation algorithm of CMEMS is not freely available and can therefore not be reproduced. However, these conclusions were drawn for the North Atlantic. Indeed, the tropics are characterized by a larger Rossby radius of deformation and therefore satellite-based eddy detection may be more successful due to larger features.

There is another approach we could use, which is not based on satellite data but on in-situ velocity measurements. This method uses observed ship data and allows us to identify eddies and their properties by one single ship track through the eddy. With an Acoustic Doppler Current Profiler (ADCP) the vessel can observe the current velocities at any time along the ship track. By applying an optimized, nonlinear damping Gauss-Newton optimization algorithm to the ADCP data, the eddy centre can be estimated and further derived properties like radius, azimuthal velocity or the Rossby number can be calculated (Castelão and Johns, 2011; Castelão et al., 2013; Bendinger, 2020).

In this study, the eddy field in the ETNA around the Cape Verde will be analysed independently using two methods based on satellite data and in-situ measurements. Then, the derived eddy parameters of both methods will be compared to detect similarities and differences. Therefore, the main research question is: Is there anything we can learn from the comparison that can help us to validate or classify satellite detected features in the future?

2. Data and Methods

2.1. Observations

The observed data from two research cruises were used for this study: M160 and M156 (Figure 1). Both cruises took place aboard the RV Meteor in 2019. M156 started on the 3rd of July and ended on the 1st of August while M160 took place from the 22nd of November to the 20th of December. Both cruises are part of the REEBUS project which focuses on the role of eddies regarding the Carbon Pump in coastal upwelling areas. Besides M156 and M160 one more cruise will take place in winter 2021. The aim of this project is to study all different types of eddies in the Canary Current System and to understand their impact on transport of bio-geochemical properties and the Carbon Pump.

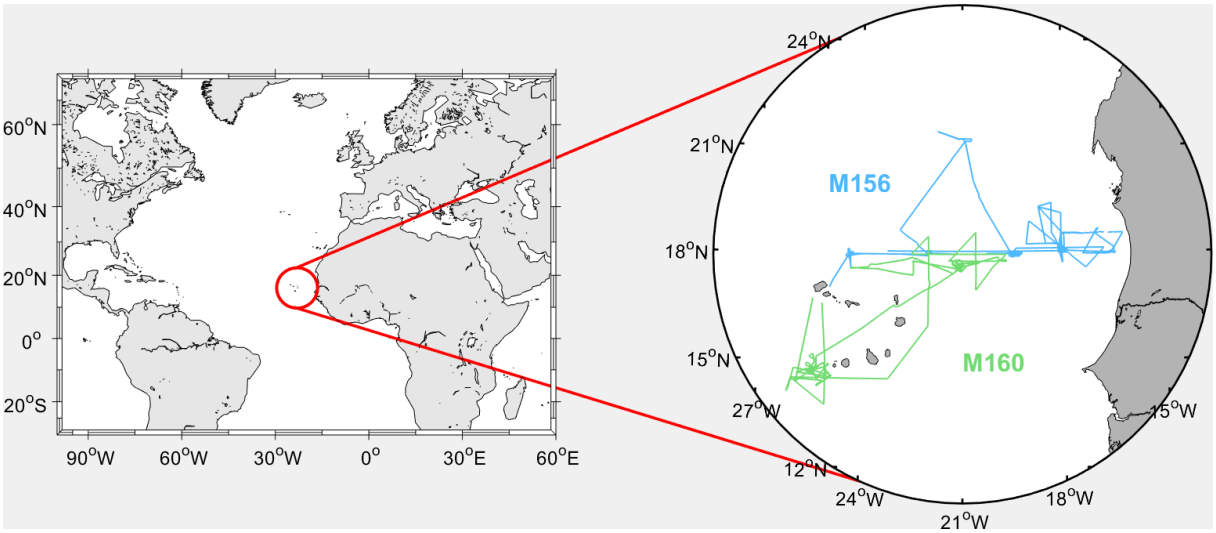

Figure 1: World map (left panel) showing position of Cape Verde islands and zoomed in map (right panel) with cruise tracks of M156 (blue) and M160 (green).

2.1.1. Vessel mounted Acoustic Doppler Current Profiler

The RV Meteor has two vessel mounted Acoustic Doppler Current Profilers (vmADCP) using 38kHz and 75kHz. This study used the 75kHz for two reasons: Due to the smaller bin size and because a systematic error occurred for the 38kHz which is not yet completely explained. The 75kHz vmADCP was configured to broad band mode with 8 m bins during M156 and the first 20 days of M160 with a depth range of 500 to 600 m. The bin size was changed on the 13th of December to 5 m bins. The averaging interval was set to one minute. The standard deviation of 1-min-averaged velocity data of a 75 kHz in broad band mode with a 8 m bin size is about 3 $^{cm}/_{s}$ (Fischer, 2011).

Further errors can occur due to the angle of installation relative to the ship's axis. The assumption for the calibration is that within a small region and short time interval the currents are constant. Therefore, changes in the absolute currents are caused by not eliminating the whole ship's speed over ground. During fast ship speeds this error is large and small when the ship is not moving. The misalignment angle and the amplitude factor try to eliminate the differences between velocity measurements when the ship is on station and not moving and when it is underway close to the station. Thus, de- and acceleration close to the station will be used as calibration points for the misalignment angle and the amplitude factor (Fischer et al., 2003).

cruise	M156	M160
misalignment angle and standard deviation	$-1.1282° \pm 0.3843°$	$-1.007° \pm 0.4869°$
amplitude factor and standard deviation	1.0033 ± 0.0095	$1.0033\pm$
number of CTD stations	59	60
$\sigma_{\overline{\alpha}}$	$0.0335°$	$0.0444°$

Table 1: Estimations for the misalignment angle and the amplitude factor with standard deviation as well as the standard error $\sigma_{\overline{\alpha}}$ of the misalignment angle with the total number of CTD stations used for its calculation.

The standard error of the misalignment angle $\sigma_{\overline{\alpha}}$ can be written as:

$$\sigma_{\overline{\alpha}} = \frac{\sigma_\alpha}{\sqrt{N}} \tag{1}$$

where σ_α is the standard deviation of the misalignment angle and N is the number of individual estimates. The number of individual estimates was measured by starts and stops for each CTD station (Table 1). Systematic errors can also occur and are more difficult to describe. Deviation of the ships compass for example can lead to different systematical errors depending on the heading. Last, the velocity was filtered by a percent-good data. Data below a threshold of 80% was neglected. Figure 2 shows a vmADCP section through an anticyclonic eddy along 13°30'N following the M160 cruise track.

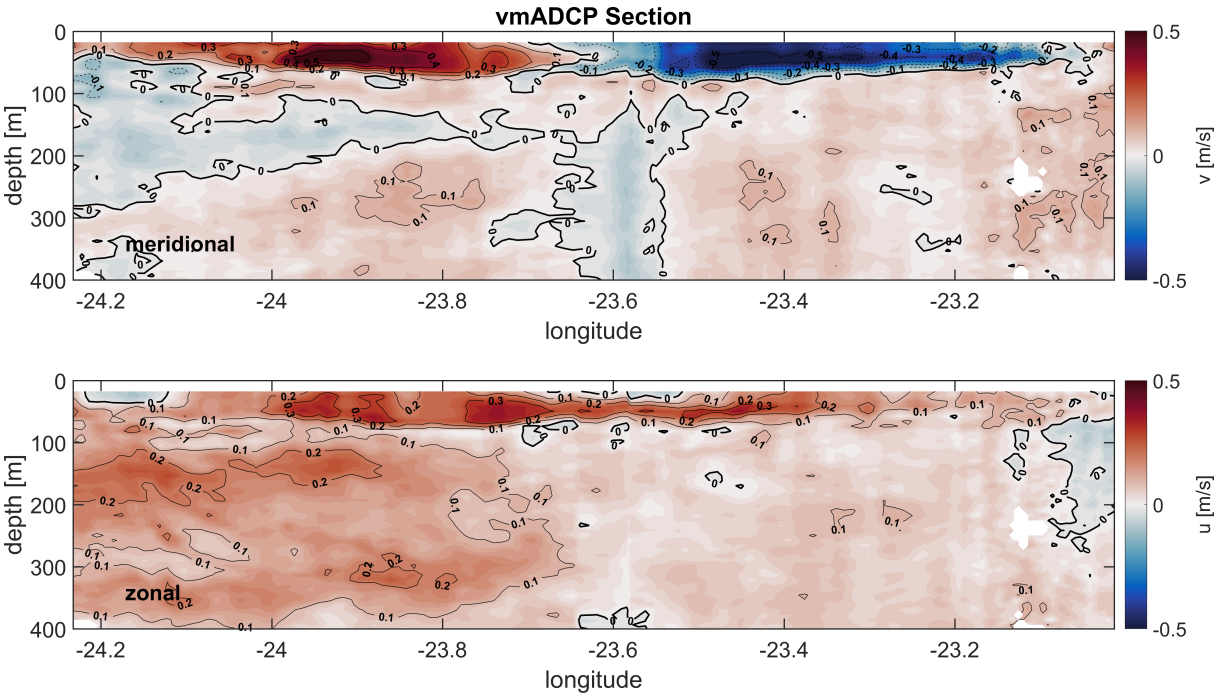

Figure 2: Smoothed and gridded 75 kHz vmADCP data showing meridional velocities (upper panel) and zonal velocities (lower panel) along 14° 30' N to the upper 400 m depth. Positive (negative) values in red (blue) represent northward (eastward) directions in m/s.

2.1.2. Sea Surface Temperature

The Thermosalinograph measures temperature and salinity continuously along the track. This data is averaged in one minute intervals. Four different sensors are measuring the temperature, where according to the user manual the best sensors on RV Meteor are sensor three and four. The data is already calibrated and compared to the CTD data in a reference depth of 5 dbar. The uncertainties for sensors three and four are ±0.002°C and ±0.004°C, respectively. Temperature and salinity measurements are available for the whole cruises.

The satellite sea surface temperature product used for this study is provided by Copernicus Marine Environment Monitoring Service (CMEMS) (global ocean - sea surface temperature multi-sensor L3 observations). It combines data from multiple satellite sensors over a 0.1° resolution grid on a daily basis in near real time. Polar orbiting (NOAA-18 and NOAAA-19/AVHRR, METOP-A/AVHRR, ENVISAT/AATSR, AQUA/AMSRE, TRMM/TMI) as well as stationary satellites (MSG/SEVIRI, GOES-11) contribute to this dataset.

2.1.3. Altimetry

The basic concept of satellite altimetry is to measure the range from the satellite to the sea surface. The altimeter transmits a pulse of microwave radiation which will be reflected by the sea surface. The range can then be calculated from the round-trip travel time of the pulse. The obtained range still varies along the satellite track due to changing sea surface topography and the distance from the orbit's height above the centre of the earth. Therefore, the knowledge of the exact position of the satellite relative to a reference ellipsoid is very important. Furthermore, other impacts which may interfere with the radar signal need to be taken into account. This can include atmospheric refraction like water vapor (Chelton et al., 2001).

The satellite product which was used for this study includes gridded and along-track sea surface heights and derived variables for the global ocean and is processed by DUACS (Data Unification and Altimeter Combination System) multimission altimeter data processing system and also provided by CMEMS (previously processed by AVISO) (Pujol et al., 2016). It is available as Level 4 data on a $1/4° \times 1/4°$ Mercator grid on a daily basis and as L3 along-track data both in near real time and delayed time. Missions that contributed to this data are: Jason-3, Sentinel-3A, HY-2A, Saral/AltiKa, Cryosat-2, Jason-2, Jason-1, T/P, ENVISAT, GFO and ERS1/2. The sea level anomaly (SLA) is computed with respect to a twenty-year mean and is defined as the difference of the sea surface height (SSH) above a reference ellipsoid and the temporal mean of the SSH over a 20 year reference period using a mean sea surface. The absolute dynamic topography (ADT) is deduced from the sum of SLA and the mean of the SSH above the Geoid over a reference time period. Therefore, the variable part of the sea surface height is shown by the SLA, while ADT displays this variable part plus the constant part averaged over a 20 year reference period (Ioannou et al., 2017). SLA tends not to represent stationary eddies which can be generated by certain bathymetry circumstances such as islands or sea mounts. Since the area where the cruises took place is characterized by islands, this study used ADT to determine the eddy field. Moreover, various studies which worked with the same algorithm used ADT instead of SLA (Ioannou et al., 2017; Le Vu et al., 2018; Garreau et al., 2018).
The CMEMS product also provides SSH derived velocities, henceforth referred as CMEMS-velocities. Due to the different satellite missions and their orbits, the return time of one satellite to a specific location can vary largely. Since the L4 satellite products are available on a daily basis, smoothing and interpolating of a few satellite tracks on spatial and temporal scale is necessary. During 29-30th of November only 4 satellite tracks crossed the region of interest (Figure 3). That visualizes the need of temporal interpolating,

especially, since those tracks are not covering the whole area.

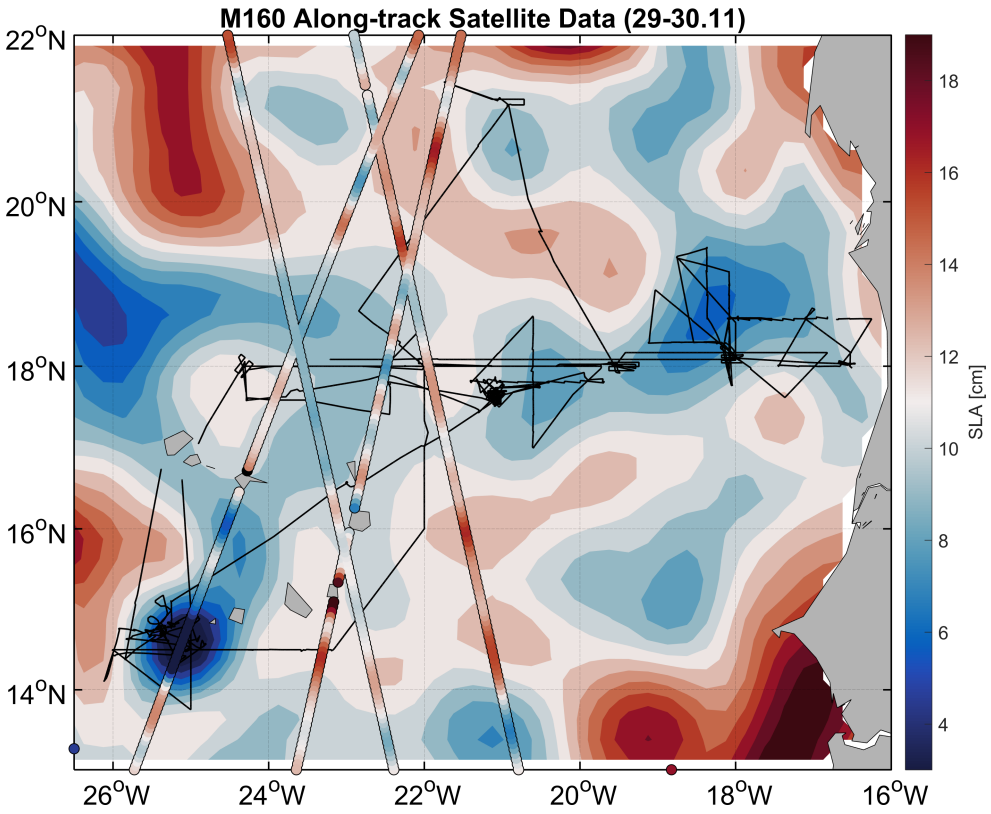

Figure 3: Gridded sea level anomaly (SLA) in cm and along-track SLA with cruise tracks of M160 and M156 as black solid line. Gridded SLA from the 30th of November and satellite tracks from 29-30.11.19.

2.2. Gauss-Newton Method

To determine the eddy field from ship-based observations, a nonlinear damping least-squares Gauss-Newton optimisation algorithm was applied to the horizontal velocity field, which was measured continuously by current profilers. This can be done by using a single ship track through the eddy. Castelão and Johns (2011) and Castelão et al. (2013) were the first who introduced this method. Following them, we assume a perfectly axisymmetric and non-translating eddy. Since working with eddies is more comfortable in cylindrical system, we will change the common Cartesian coordinates into cylindrical coordinates. There, the xy coordinates correspond to a radial vector and an azimuthal angle. Now we can distinguish between the radial v_r and azimuthal v_θ velocity. The total velocity V can be written as the sum of the radial and azimuthal component:

$$\vec{V} = \vec{v_r} + \vec{v_\theta} \tag{2}$$

The radial component is always directed to the outer edge of the eddy while the azimuthal velocity is tangential to the eddy's rim. Based on the axisymmetric and non-translating eddy, all the momentum should be contained in the azimuthal velocity or in other words, the radial component should strive towards zero.
To get to the relation of $V(r)$, we need to have an accurate eddy centre estimation, which we will achieve by applying the nonlinear damping least-squares Gauss-Newton optimisation algorithm. This algorithm estimates the location of the centre by minimizing the difference between the total velocity and the azimuthal component, since the centre is the point where the azimuthal component is largest or the radial component smallest. Essentially, it is an iterative procedure, which finds the pair of coordinates which fits the assumption of a minimal radial velocity component best. The minimization is performed by applying the least-squares method to an objective function. The Gauss-Newton method can be written as:

$$\vec{V} = -u \sin\theta + v \cos\theta + \epsilon \tag{3}$$

$$\theta = \arctan(y_r / x_r) \tag{4}$$

$$y_r = y - y_c \tag{5}$$

$$x_r = x - x_c \tag{6}$$

where V is the total velocity, x and y are the positions of the velocity sample along the ship track, x_c and y_c are the positions of the estimated eddy centre and ϵ is the residual measuring the discrepancy between the objective function and the observational data. When the eddy was crossed entirely, the ship track will be separated in two radial sections

which will be analysed separately. The final eddy centre estimate will then consist of the mean of all previous estimations.
Since nature is not always as perfect as the assumption expects, a background flow can lead to noisy samples near the rim of the eddy (Castelão and Johns, 2011). These can be excluded by a second iterative procedure. Castelão et al. (2013) also stated that the translational speed of a propagating eddy can not be neglected. They showed that if the translation was neglected, errors up to 30 km can occur for a North Brazil Current Ring of 160 km radius. Others argued that if the sampling of the eddy only took a short time comparing to the translating speed, one can consider not to correct the velocities as the influence may be unrecognizable small (Bendinger, 2020). Once the centre estimation is done, one can calculate derived characteristics such as maximum azimuthal velocity, radius, sea surface height footprint, inner core vorticity and the decay scale. For further information regarding the Gauss-Newton method see Bendinger (2020).

Still, there are some disadvantages. On the one hand, Bendinger (2020) showed that the estimated variables highly depend on the location of the ship track through the eddy. One can achieve the best results if the ship track is crossing through the centre as close as possible. This can pose challenges, since the real eddy centre is in most cases unknown at the beginning. To get good estimations, it is also important that the eddy is crossed entirely, so the decay of the velocity is displayed as well. Otherwise the calculation of the decay scale can have large uncertainties.
In addition, Castelão and Johns (2011) showed that for good and trustworthy estimations, it is best to have several sections through the eddy. Individual sections will be analysed independently and the results will be averaged to get to the final estimation.
Furthermore, the Gauss-Newton method can not give any information regarding the asymmetry of an eddy, due to the assumption of a perfectly axisymmetric vortex.

Despite of these limitations, this method allows a precise estimation of mesoscale eddies and their parameters by using just one ship track. Bendinger (2020) did a skill assessment and applied the method to artificial cruise tracks from a high resolution model (NATL60). He showed that most of the derived properties lie within 10% and just inner core vorticity and the decay scale lie within 20%. Therefore, this study will take the results from this method as ground truth and compare the satellite derived parameters with its results.

2.2.1. Azimuthal velocity, radius and outer ring decay scale

Once the eddy centre is determined, one can derive eddy describing parameters such as maximum azimuthal velocity, radius or outer ring decay scale (Figure 4).

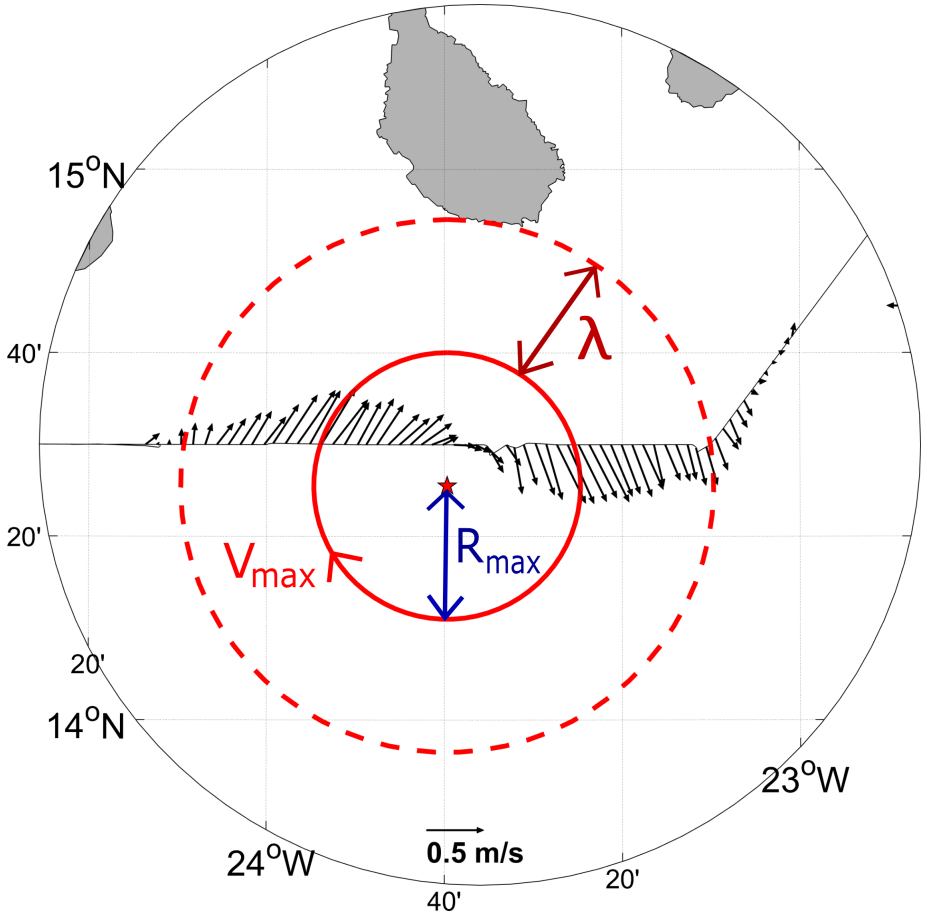

Figure 4: Eddy properties derived from the Gauss-Newton method where black arrows display the vmADCP data.

As introduced above, an ideal, axisymmetric and non-translating eddy is the fundamental assumption. Therefore, one can define the velocity of an ideal eddy as follows:

$$v_\theta(r) = \begin{cases} r\frac{V_{max}}{R_{max}} & \text{for } r < R_{max} \\ V_{max}e^{-\frac{r-R_{max}}{\lambda}} & \text{for } r > R_{max} \end{cases} \tag{7}$$

Where V_{max} is the maximum azimuthal velocity and R_{max} is the distance from the eddy centre to the maximum azimuthal velocity, r is the distance to the centre and λ is the e-folding scale. The inner core ($r < R_{max}$) of an ideal vortex follows the solid body rotation. This signifies that the velocity is increasing linearly with increasing radius. In the outer ring ($r > R_{max}$) the velocity is decreasing exponentially (Castelão and Johns, 2011; Olson, 1991).

2.3. AMEDA

This study uses the Angular Momentum Eddy Detection and Tracking Algorithm (AMEDA) to detect eddies and their properties from altimetric data (Le Vu et al., 2018). Unlike other common automatic tracking algorithms, AMEDA combines two different approaches. It is based on dynamical parameters as well as geometrical properties of the velocity field. The first dynamical parameter is called Local Normalized Angular Momentum (LNAM). This method was built to distinguish between hyperbolic and elliptical points and was first introduced by Mkhinini et al. (2014). They compute the angular momentum for a local area. Due to the normalization, the parameter reaches an extremum in the core of the eddy. The value would either be +1 or -1 depending on the sense of rotation of the eddy: cyclonic or anticyclonic, respectively (Le Vu et al., 2018). Once the centres are detected, a second dynamical parameter will be applied: The local Okubo-Weiß (LOW) parameter. This will make sure that only centres, which are in vorticity dominated regions are taken into account.
The Okubo-Weiß parameter OW distinguishes between deformation and rotation and can be written as:

$$OW = s_n^2 + s_s^2 - \omega^2 \tag{8}$$

where $s_n = (\partial u/\partial x) - (\partial v/\partial y)$ is the normal strain, $s_s = (\partial v/\partial x) + (\partial u/\partial y)$ is the shear strain and $\omega = (\partial v/\partial x) - (\partial u/\partial y)$ is the relative vorticity (Schütte et al., 2016). For the core of an eddy the OW will reach negative values since it is dominated by vorticity (Le Vu et al., 2018). The local Okubo-Weiß is hence the OW applied to a local area - here the same area where the LNAM was computed. Only if the LOW shows negative values, the centre will be contained in the analysis.
Since the LNAM maxima and the LOW still can not guarantee that the detected centre belongs to a water masses trapping eddy, a geometrical parameter will be applied. Therefore, an eddy centre will only be kept if it has a closed streamline surrounding it (Le Vu et al., 2018).
Several derived variables can be calculated such as maximal and mean azimuthal velocity, radius or the Rossby number. The closed streamline with the maximum azimuthal velocity will be called characteristic contour which corresponds to R_{max} (Figure 8). AMEDA is able to work with either ADT or SLA. SLA represents the variable part of the Sea Surface Height while ADT consist of the variable part plus the constant part averaged over a 20 year reference period (Ioannou et al., 2017). Therefore, stationary features are averaged out by using SLA. Since the region of interest is characterized by islands as well as sea mounts, stationary features are quite possible. Furthermore, several studies that worked with AMEDA used ADT instead of SLA (Le Vu et al., 2018; Ioannou et al., 2017;

Garreau et al., 2018). Hence, the choice for this study regarding the altimetric product fell on ADT.

Le Vu et al. (2018) stated that AMEDA is robust to grid resolution and can hence be applied to various fields with different spatial resolutions. AMEDA also comes with a minimal number of tunable parameters which makes it user-friendly. Besides, the characteristic contour gives an idea of the shape of the eddy and the algorithm can offer information regarding the complete dynamical evolution of eddies. Furthermore, merging and splitting events can be identified (Le Vu et al., 2018). AMEDA was used before to detect eddy characteristics. Aroucha et al. (2020) applied the algorithm with the intention to analyse North Brazil Rings in the western tropical North Atlantic. They were interested in the lifetime, maximal radius, maximal azimuthal velocity, Rossby radius of deformation and eddy kinetic energy as well as the Sea Surface Height anomaly. AMEDA was also used to study eddies in the Mediterranean Sea (Ioannou et al., 2017) and in the Algerian Basin (Garreau et al., 2018). Since AMEDA can work best on a fine grid resolution, eddy estimations based on the coarse global CMEMS grid resolution of $1/4° \times 1/4°$ can contain errors. Le Vu et al. (2018) showed that for this resolution AMEDA can not guarantee valid information for $R_{max} < 50$km. Nevertheless, since the global CMEMS data set is the best altimetric product for that region, AMEDA will be applied despite the sensibility to the coarse grid resolution.

2.4. Rossby Number

The Rossby Number Ro is a dimensionless number which determines the importance of the Coriolis force with respect to local advection. Ro is defined as

$$Ro = \frac{U}{fL} \tag{9}$$

where L is the length scale, U the velocity scale and f the Coriolis parameter. Ro in case of an eddy can also be written as:

$$Ro = \frac{V_{max}}{fR_{max}} \tag{10}$$

Small values of the Rossby number $Ro \lesssim 0.2$ indicate a flow which is dominated by the Coriolis force such as large-scale planetary flows, while values closer to 1 indicate that the local advection is more important than the Coriolis acceleration. Schütte et al. (2016) showed that for typical length and velocity scales of eddies the Rossby number is close to 1.

Furthermore, the Rossby number is an indicator for nonlinearity of the flow regime. Large Rossby numbers represent an increasing importance of the nonlinearity. Nonlinear eddies are characterized by a greater rotational than translational speed, non-linearity also separates eddies from linear waves. Chelton et al. (2011b) stated that nonlinear eddies have the ability to trap fluid inside of their cores as they propagate. With increasing non-linearity, the local advection gains more importance and therefore the centrifugal force has to be taken into account. This leads to cyclo-geostrophic balance rahter than geostrophic balance. The centrifugal force is always directed radially outward, cyclonic eddies present with a higher sea surface slope compared to geostrophic cyclones. The sea surface slope of anticyclones would be relatively smaller than their geostrophic opponents. Features with a high surface elevation can be better detected and characterized by satellite data, since that is the subject of measurement.

3. Results

3.1. In-situ Measurements derived eddy characteristics

When the nonlinear damping least-squares Gauss-Newton optimization algorithm was applied to the vmADCP data, five eddies were found during the M156 cruise and three during M160 (Figure 5).

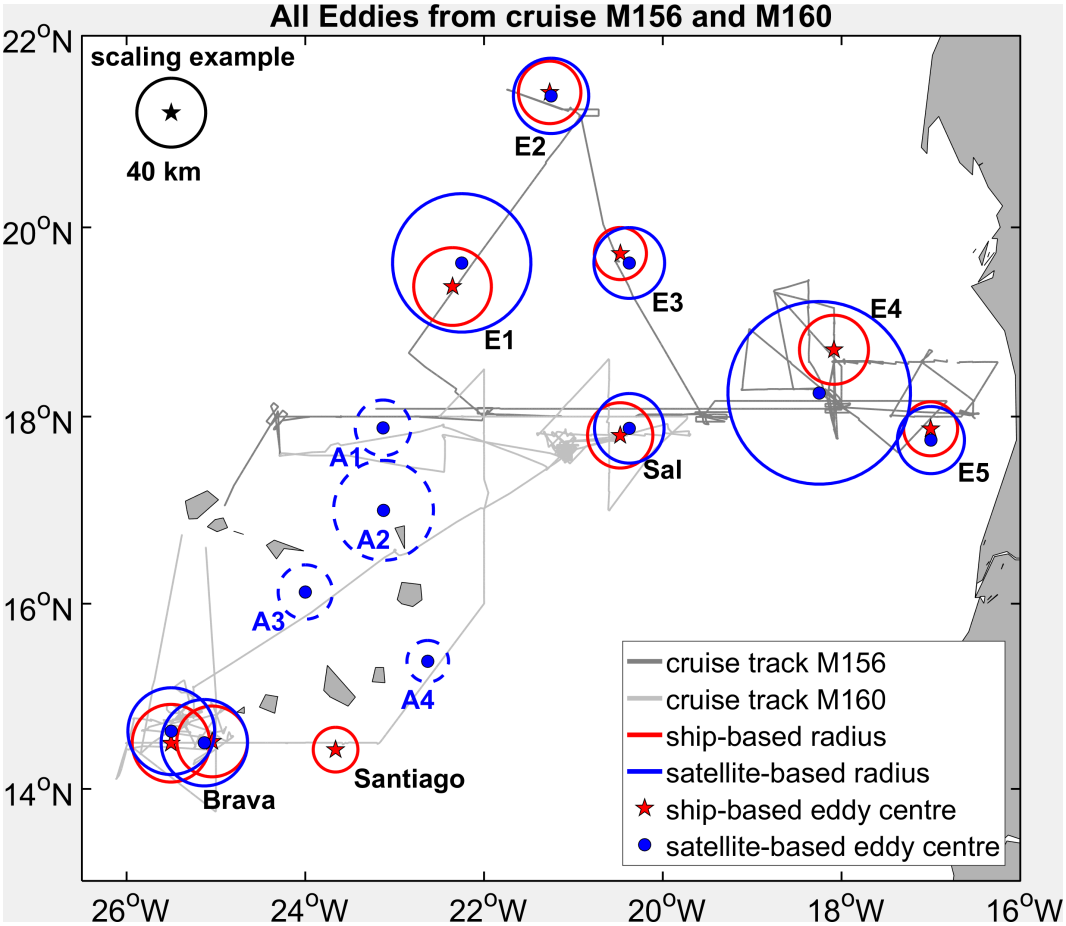

Figure 5: Map of the area of Cap Verde Islands with cruise tracks of M156 and M160 in dark and light grey, respectively. Circles marking radius of maximum azimuthal velocity of ship-based (red) and satellite-based (blue) methods with stars and points representing the centre, respectively. Eddies which were only found by the satellite-based method are visualized by dashed lines.

Even though the vmADCP (75kHz) can reach down to about 500-600 m depth, for this estimations the velocities of the upper 17.5 to 50 m were averaged. Since this study aims to compare results with estimates from satellite data, which just represent the ocean's surface, only surface velocities are of interest. But then, using only the first bin of the vmADCP with a mean depth of 17.5 m other problems will arise. First, the upper metres can suffer from noise such as ship movement. Second, the upper ocean can also experience

acceleration due to external forces such as wind stress. A few hours of strong wind blowing on the ocean, can lead to surface currents which are only affected by the Coriolis force, so called inertial currents (Von Arx and Dwight, 1962). To avoid only displaying velocities of external forces rather than velocities caused by eddies, the depth range of 17.5-50 m was chosen. Therefore, it is assured that the motion of the upper ocean is represented with less noise due to local, short time wind events.
In the following, the names next to the circles in Figure 5 will be used to refer to a specific eddy.
Brava is the only eddy which was surveyed two times, in the beginning and at the end of the cruise. Hereafter, it will be referred to as either Brava 1 or Brava 2 for the first or the second survey, respectively. If an eddy was crossed more than once, all estimations from the individual sections were averaged. The results are displayed with their standard deviations in Table 2.

Gauss-Newton derived Eddy Parameters					
Eddy Nr/Name	R_{max} [km]	V_{max} [cm s^{-1}]	λ [km]	Ro	type
E1	45.7	27.70	37	0.13	Anticyclone
E2	36.51 ± 0.4	29.75 ± 2.9	32.99	0.15 ± 0.01	Anticyclone
E3	30.38 ± 1.8	46.84 ± 2.8	23.40	0.33 ± 0.02	Anticyclone
E4	40.72 ± 11.6	24.3 ± 5.60	47.2 ± 38.6	0.13 ± 0.009	Cyclone
E5	32 ± 6.8	38.3 ± 4.60	31	0.28 ± 0.02	Anticyclone
Brava 1	42.67 ± 11.3	40.31 ± 0.6	33 ± 4	0.27	Cyclone
Brava 2	46.83 ± 0.86	36 ± 6.4	33 ± 4	0.21	Cyclone
Santiago	27 ± 2.1	49.5 ± 2.4	53.9 ± 25.4	0.51± 0.06	Anticyclone
Sal	38.7 ± 3.4	19.8 ± 0.07	40 ± 15	0.13 ± 0.04	Cyclone
Mean	37.23 ± 7.1	34.02 ± 10.4	39 ± 12	0.24 ± 0.13	-

Table 2: Eddies from M156 and M160 with their mean properties and standard deviations. For eddy names compare Figure 5, R_{max} is the radius of maximal azimuthal velocity and V_{max} is maximal azimuthal velocity, λ is the decay scale and Ro the Rossby number. Type describes the sense of rotation: Anticyclones and Cyclones rotate clockwise and counterclockwise, respectively.

The radius of maximum azimuthal velocity of all eddies was on average 37 km with a standard deviation of 7 km. The mean maximum azimuthal velocity was 34 $^{cm}/_{s}$ with a standard deviation of 11 $^{cm}/_{s}$ (table 2 for all eddies and their properties). The Santiago Eddy was found to be the smallest but fastest with $R_{max} = 27 \pm 2$km and $V_{max} = 49.5 \pm 2.4^{cm}/_{s}$. Brava 2 has the largest R_{max} with about 47 km and Sal the smallest maximum azimuthal velocity with only 20 $^{cm}/_{s}$. The decay scale λ varies between 31 and 54 km, but this property needs to be handled with care. A good estimation for λ

depends highly on the section through the eddy and can only be considered reasonable if the section covers the whole maximum until the velocity is completely decreased. The Rossby numbers vary between 0.13 (E1 and Sal) and 0.51 (Santiago) with a mean value and standard deviation of 0.24 ± 0.13.

Some eddies (Brava, Sal, E4 and E5) were crossed several times which strengthens the estimation and gives a more complete picture of the eddy (Figure 6).

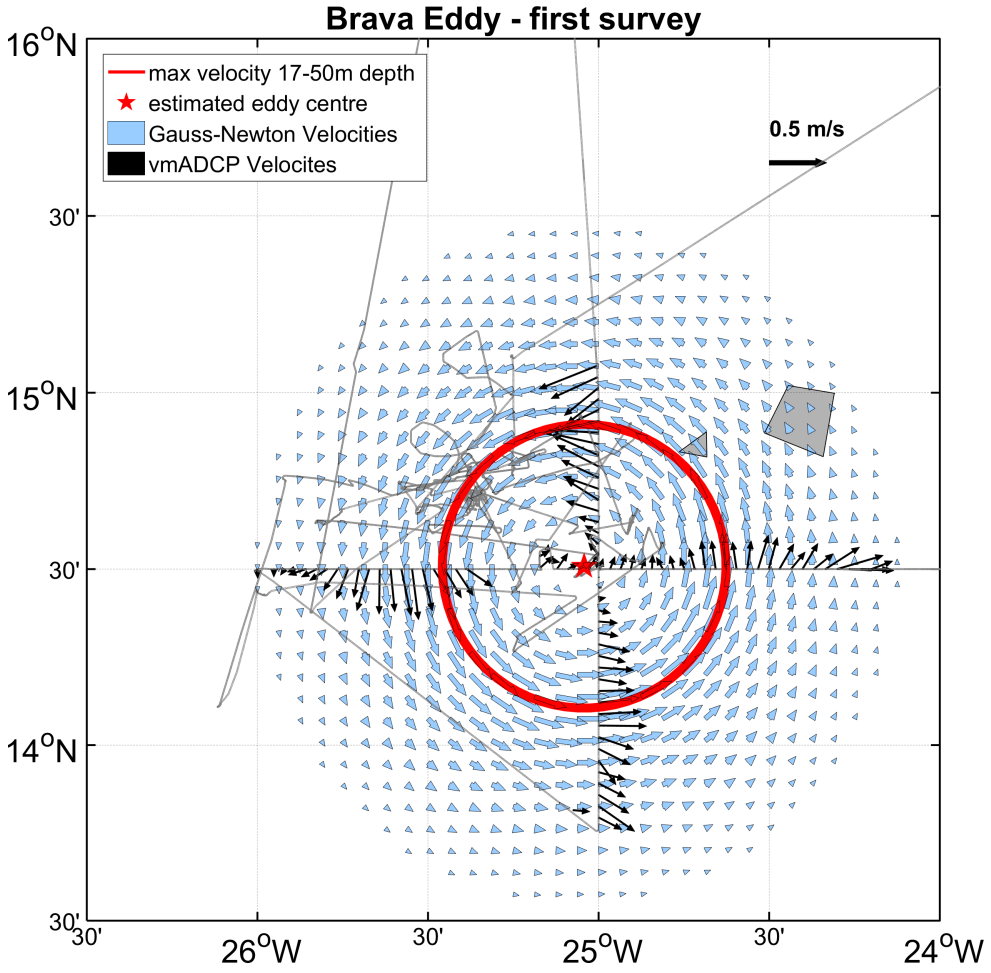

Figure 6: Brava 1: Estimated velocities of the upper ocean 17.5-50 m (blue arrows), R_{max} = 43km and V_{max} = 40$^{cm}/_{s}$ in red and centre as a red star, vmADCP velocities of the upper 17.5-50 m depth (black arrows).

Still, the Gauss-Newton method highly depends on the location of the ship track through the eddy (Figure 7). Dislocated ship tracks can cause high variations of the eddy size and can be even more severe if there is a combination of two close-by eddies. The velocity maxima of both eddies can combine to a larger one which can differ over 50% from the real eddy (Figure 7). Therefore, the closer the ship track is to the centre the more reliable is the eddy centre estimation and the derived variables.
This is also confirmed by Bendinger (2020).

Nonetheless, crossing the eddy through its real centre can be challenging since the exact

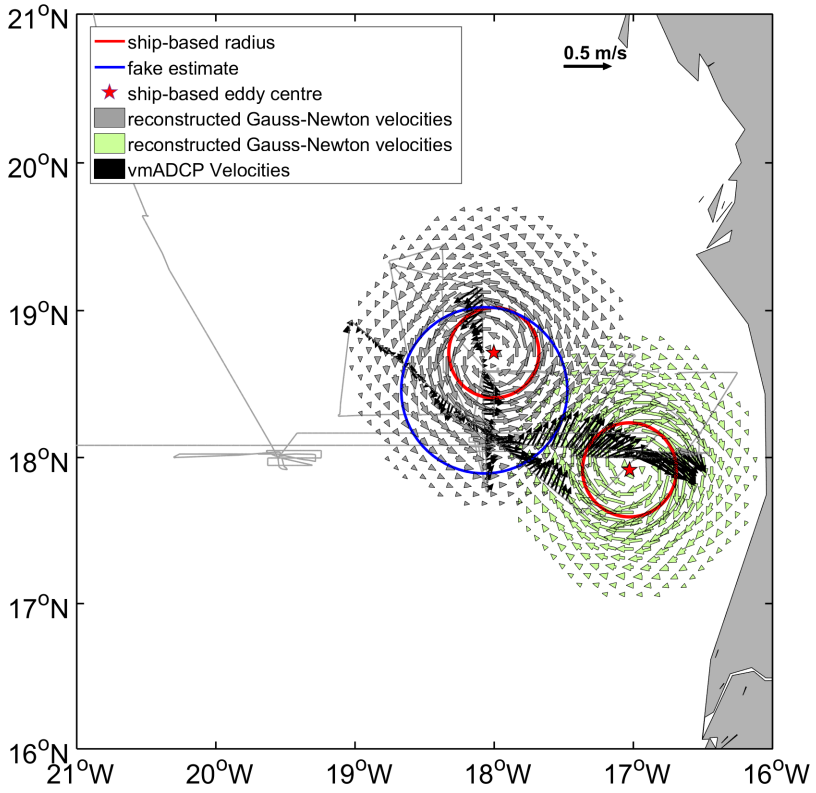

Figure 7: Ship-based estimates of E4 and E5 with radius and centre in red, the reconstructed velocity field from eq. (7) in grey and green with corresponding vmADCP velocities visualized by black arrows. The blue circle illustrates that ship tracks which are not crossing the centre can cause false estimations.

location of an eddy is unknown in the beginning. It only can be estimated by using satellite products which are often overestimating the radius and hence dislocate the centre.
Another difficulty is that there are sometimes more than two velocity maxima found during one crossing as a result of the deformation and inhomogeneity of the eddy. This can yield to false estimations. Also shown by Bendinger (2020), the algorithm can not determine whether it found a local or global minimum by minimizing the objective function and stick with it no matter what.
The Gauss-Newton method also does not give any evidence on the asymmetry of the eddy since it assumes a perfectly axisymmetric vortex. The final estimate also highly depends on the initial conditions, therefore Bendinger (2020) introduced a cluster of start values to make sure that those values are in a good range. Using in-situ measurements of the velocity field, one should consider further problems that may occur. There are other factors which can contribute to the velocity field such as tides, a mean flow, coastal currents or the translational speed of the eddy (which also can be caused by the mean flow e.g.). These factors can cause deformation and inhomogeneity which can lead to

deviating estimates of eddy characteristics.

Furthermore, the method does not take the propagation of the eddy into account. Schütte et al. (2016) showed that eddies in the eastern tropical North Atlantic propagate with a mean speed of $3 \pm 2.15 {}^{\mathrm{km}}/_{\mathrm{day}}$. Assuming that a survey consisting of a meridional and zonal section took two to three days during M160 and the eddy propagates with the mean speed of 3 ${}^{\mathrm{km}}/_{\mathrm{day}}$ the eddy would have travelled 6 to 9 km. With a mean radius of 37 km the eddy would have travelled 16% (2 days) or 24% (3 days) of its radius during the survey. One could consider that amount to be not negligible and could correct the measured velocities regarding the speed of propagation. Even if the time of the survey is for most of the eddies (Santiago, E1-E3, E5) shorter than two or three days due to a single crossing, there are eddies where the survey even took several additional days. The survey of Brava 2 and Sal provided additional sections due to the investigation of fronts near the rim of the eddy which in some cases took place several days after the main survey. Castelão et al. (2013) also states that in most cases a correction of the measured velocity field regarding the propagation speed is necessary as the caused errors can not be neglected. The measured velocities consist of the westward translational and the rotational speed of the eddy. This can be illustrated by a meridional section through the eddy. Measured westward velocities seem to be stronger while eastward velocities are weaker compared to a perfect eddy. Especially for eddies with low azimuthal velocity when the propagation speed is large in comparison to the rotation, a correction of the velocities is important. Concluding, one can say that a correction of the velocities for eddies with a long survey period and small azimuthal velocities is reasonable or even necessary.

3.2. Satellite derived eddy characteristics

AMEDA was the method of choice to determine eddies from satellite products for this study (Figure 8). AMEDA was applied to each cruise for the whole time period.

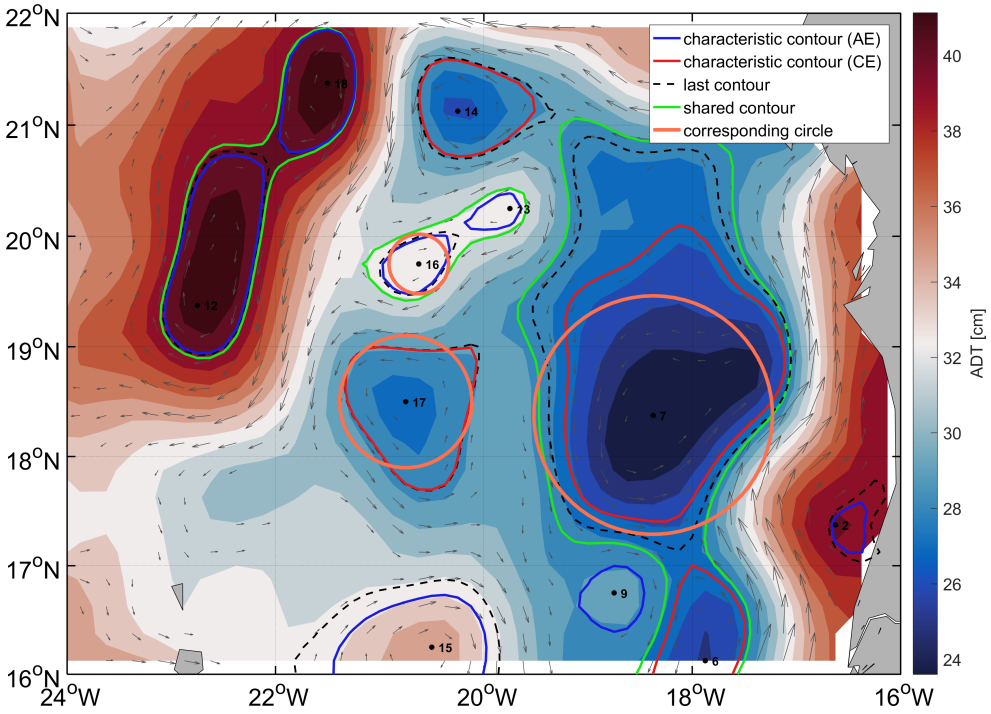

Figure 8: Snapshot of eddy field identified by Angular Momentum Eddy Detection and Tracking Algorithm (AMEDA). Cyclones and Anticyclones are colored in red and blue, respectively. Characteristic contours mark the closed streamline which corresponds to the maximum azimuthal velocity, if the last closed contour differs from the characteristic contour it is marked as a black dashed line. Shared contours are marked in green. Eddy centres are displayed with a dot and a number corresponding to the total number of eddies found in that area that day.

The number and size of eddies that were detected vary on a daily basis. Since the intention of this study is to compare AMEDA to the ship-based measurements, only the time period during a survey of one certain eddy was used to determine the eddy characteristics with AMEDA for that eddy of interest. That is important to guarantee the comparability of the results to the in-situ measurements, which only take a snapshot of the eddy during the survey.

With one exception, all the eddies described through the ship-based method could be found with the AMEDA analysis of the gridded ADT maps as well (Figure 5). The Santiago eddy did not occur in the AMEDA analysis of the same day as the ship crossed that area.

Furthermore, AMEDA detected eddies close to the ship track or even crossed by it which could not be detected by the in-situ velocity measurements.
Characteristics of eddies close to the cruise tracks are shown in Table 3. Mean values exclude features A1-A4. Note that R_{max} is the equivalent radius of a circle with the same surface area as the characteristic contour.

AMEDA derived Eddy Parameters				
Eddy Nr	R_{max} [km]	V_{max} [cm s^{-1}]	Ro	type
E1	81.2 ± 3.1	14.58 ± 0.01	0.04	Anticyclone
E2	43.7 ± 0.4	14.11 ± 0.01	0.06	Anticyclone
E3	41.5 ± 20	8.5 ± 2.8	0.04	Anticyclone
E4	108 ± 15.5	14.42 ± 0.8	0.03	Cyclone
E5	39.8 ± 1.5	15.08 ± 0.4	0.09	Anticyclone
Brava 1	52.1 ± 0.8	37.12 ± 0.7	0.2	Cyclone
Brava 2	52.3 ± 1.5	37.5 ± 0.7	0.19	Cyclone
Santiago	-	-	-	Anticyclone
Sal	41.2 ± 9.4	7.02 ± 1.3	0.04	Cyclone
A1	33	4.3	0.03	Anticyclone
A2	60	6	0.02	Cyclone
A3	32.5	4.5	0.03	Anticyclone
A4	25	4	0.04	Cyclone
Mean (without A1-A4)	61.6 ± 26.2	18.54 ± 11.97	0.08 ± 0.06	-

Table 3: Shows Eddies from M156 and M160 with their mean properties and standard deviations. For eddy names compare Figure 5, R_{max} is the radius of maximal azimuthal velocity, V_{max} is maximal azimuthal velocity and Ro the Rossby number. Type describes the sense of rotation: Anticyclones and Cyclones rotate clockwise and counterclockwise, respectively.

For following descriptions and averages, eddies A1-A4 are not taken into account since they could not be confirmed by ship measurements. A1-A4 will be investigated later in this study. The mean radius of maximum azimuthal velocity was 44.2 km with a standard deviation of 3.4 km.
The mean maximum azimuthal velocity counts 9.2 $^{cm}/_{s}$ with a standard deviation of 0.9 $^{cm}/_{s}$. Only estimates during the days of the surveys contributed to the individual values. If one just averages the radii and velocities of the eddies which were also detected by using in-situ velocity measurements and only takes the days corresponding to the time period of the surveys into account, the results show a greater R_{max} with 61.6 ± 26.2km and V_{max} with $18.5 \pm 12^{cm}/_{s}$ with nine and twelve times greater standard deviation compared to the mean over the whole time period and all AMEDA detected eddies. The Rossby number Ro ranges between 0.03 (E4) and 0.2 (Brava 1) with an average of 0.08 and a standard

deviation of 0.06. A1-A4 presented with smaller radii (except for A2), smaller velocities as well as smaller Rossby numbers.

3.3. Comparison of ship-based and satellite-based results

The comparison of satellite derived eddy characteristics to the in-situ measurements of the velocity field is divided into three main parts. First, eddies and their characteristics which were found with both methods will be compared. The second part will focus on eddies which were present in the surface velocity data but were not detected by satellite-based method. Finally, eddies that were found by the gridded ADT maps and crossed by the ship tracks of the cruises but which could not be detected within the surface velocity field of the vmADCP will be analysed.

Starting with the eddies which were detected by both algorithms, there are seven eddies in total. The derived parameters can be found in table 4. As an additional information in this table the column *differences* was added. It shows how much the satellite estimates differ from the ship-based measurements in percent.

Comparing the radii one can see that satellite products except for one eddy (Sal) overestimate the radii. The difference in percent indicates that radii estimated by the satellite-based method are about 68% larger than those estimated by in-situ measurements. They range between 5% and 163% causing a high standard deviation of 53%. The maximum azimuthal velocity is also varying broadly. In average, estimates using satellite products are 45% smaller than the estimates based on ship-measured velocities. The difference ranges between 8% and 82% with an a relatively high standard deviation of 30%. In most cases the Rossby numbers tend to be highly underestimated up to 87% by the satellite method.

Comparing the results one can divide the satellite estimates roughly into three categories. First, eddies with good estimates for R_{max} and V_{max}. Both estimations for the Brava eddy fit in that category. Indeed, those are the only good estimations for V_{max}. In addition, the Rossby number for Brava 2 is very well estimated (7% smaller) while for Brava 1 (41%), it is still better than estimations of other eddies.
Second, eddies with a relatively good radius estimation but a weak estimation for V_{max} will be sorted into category two. Sal, E3 and E5 have these criteria.
What remains are radii estimations which differ largely from the ship-based estimates. Radii from E1 and E4 differ 76% and 163% from the in-situ measurements derived estimates, respectively. In conclusion, satellite products tend to overestimate horizontal length scale while the velocity and non-linearity (based on Ro) are underestimated. By applying the radii estimations against each other, it is clearly visible that satellite-based estimates are almost always larger than ship-based estimates (Figure 9, left panel). Furthermore, no correlation can be found for large values of R_{max}.

Comparison of AMEDA and Gauss-Newton derived Eddy Parameters					
Eddy	parameter	Gauss-Newton	AMEDA	difference [%]	type
E1	R_{max}	45.7	81.17 ± 3.1	76	Anticyclone
	V_{max}	27.7	14.58 ± 0.01	47	
	Ro	0.13	0.04	71	
E2	R_{max}	36.5 ± 0.4	43.69 ± 0.4	19	Anticyclone
	V_{max}	29.8 ± 2.9	14.11 ± 0.01	56	
	Ro	0.15 ± 0.01	0.06	59	
E3	R_{max}	30.4 ± 1.8	41.51 ± 20	36	Anticyclone
	V_{max}	46.8 ± 2.8	8.5 ± 2.8	82	
	Ro	0.33 ± 0.02	0.04	87	
E4	R_{max}	40.7 ± 11.6	108 ± 15.5	163	Cyclone
	V_{max}	24.3 ± 5.6	14.42 ± 0.78	41	
	Ro	0.13 ± 0.01	0.03	78	
E5	R_{max}	32 ± 6.8	39.82 ± 1.5	25	Anticyclone
	V_{max}	38.3 ± 4.6	15.08 ± 0.4	61	
	Ro	0.28 ± 0.02	0.09	70	
Brava 1	R_{max}	42.7 ± 11.3	52.09 ± 0.8	21	Cyclone
	V_{max}	40.3 ± 0.27	37.12 ± 0.7	8	
	Ro	0.27	0.16	41	
Brava 2	R_{max}	46.8 ± 0.9	52.3 ± 1.5	11	Cyclone
	V_{max}	36 ± 6.4	37.5 ± 0.7	3	
	Ro	0.21	0.19	7	
Sal	R_{max}	38.7 ± 3.4	41.24 ± 9.4	5	Cyclone
	V_{max}	19.8 ± 0.07	7.02 ± 1.3	67	
	Ro	0.13 ± 0.04	0.05	64	
Mean	R_{max}	37.23 ± 7.1	61.6 ± 26.2	68	-
	V_{max}	34.02 ± 10.4	18.54 ± 11.97	44	-
	Ro	0.24 ± 0.13	0.08 ± 0.06	67	-

Table 4: Eddies from M156 and M160 with their mean properties and standard deviations. For eddy names compare Figure 5, R_{max} is the radius of maximal azimuthal velocity, V_{max} is maximal azimuthal velocity and Ro is the Rossby number. Type describes the sense of rotation: Anticyclones and Cyclones rotate clockwise and counterclockwise, respectively.

Nevertheless, investigating radii between 40-60 km, one can see a correlation. With increasing ship-based radius, the satellite estimations also increase. No pattern regarding cyclonic or anticyclonic rotation can be found. Also worth mentioning is that no satellite-based radius is smaller than 40 km. Satellite-based velocity estimates are, except for one, always smaller than ship-based velocities (Figure 9, right panel). No relation can be determined. Noteworthy is that the only good estimates have large values of 37 $^{cm}/_{s}$ and belong to Brava 1 and 2.

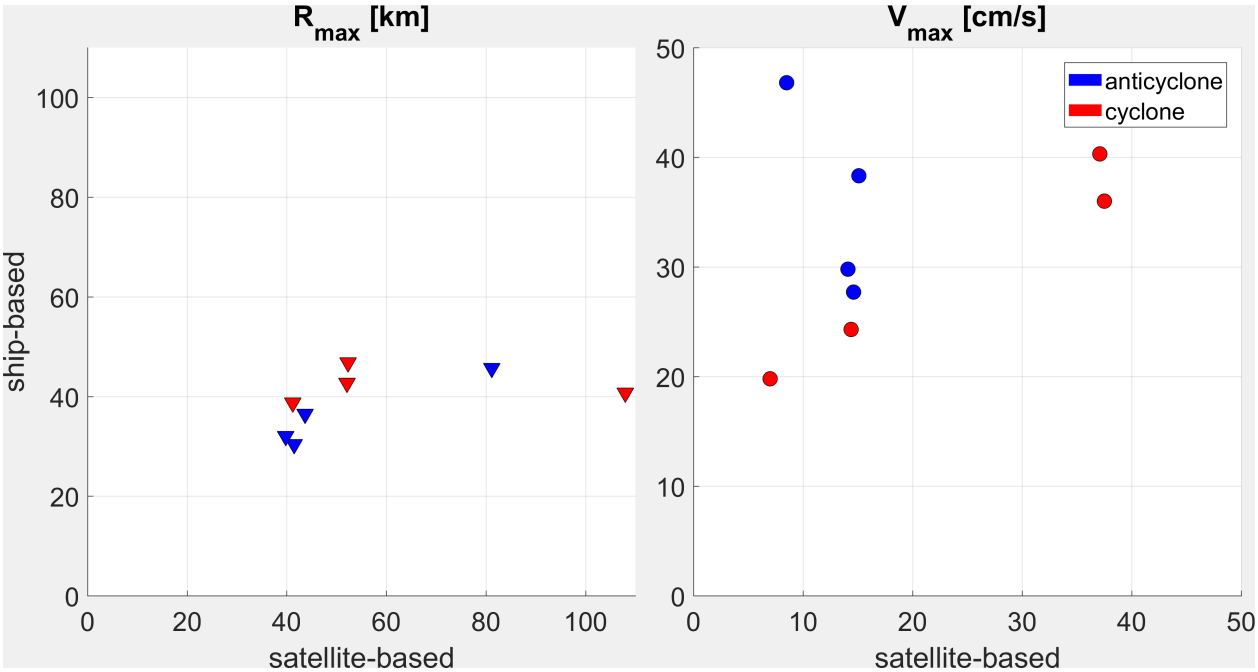

Figure 9: Satellite and ship-based radius and maximum azimuthal velocity. Blue (red) colors mark anticyclones (cyclones).

Again, no further conclusion can be drawn for the distribution of cyclones and anticyclones.

To determine further correlations, the Rossby number was compared to the differences of V_{max} and R_{max}. Estimations with large Rossby numbers (close $Ro = 0.2$) provide good results with only small differences. These estimations belong to the Brava eddy which was detected as a strong cyclone. Large values of the Rossby number indicate a strong influence of local advection and therefore centrifugal force gains importance. Consequently, cyclones have a higher sea surface slopes when describing them with cyclo-geostrophic balance rather than with geostrophy. As satellites measure the sea surface height, larger sea surface slopes are better detectable and therefore better estimations can be expected. This theory is confirmed by the estimations of the Brava eddy.
Focusing on the remaining radii in comparison with the Rossby number, two additional conclusions can be drawn. First, good estimates appear for Rossby numbers larger than 0.05. When the Rossby number drops below 0.04 no valid information can be derived since there are some estimates with low differences and some differ up to 160%. Moreover, the Rossby numbers of A1-A4 presented with small values ranging between 0.02-0.04 that strengthens the hypothesis of estimates with $Ro < 0.04$ can be declared as a false detection.
V_{max} shows a similar behavior for large Rossby numbers which also underlines the hy-

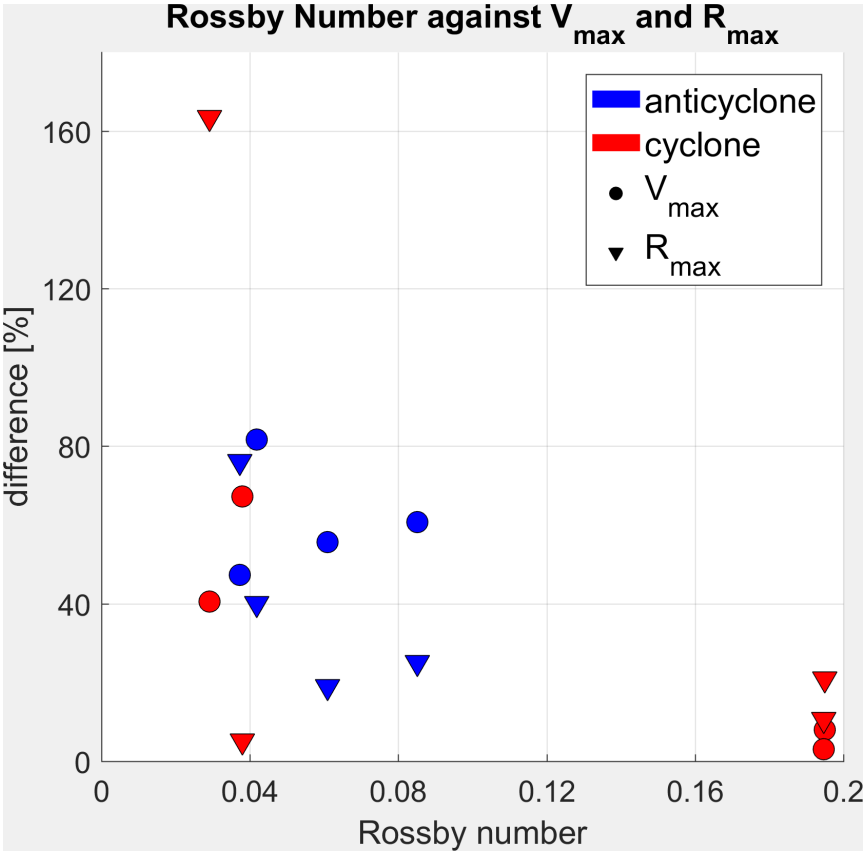

Figure 10: Satellite-based Rossby number against the difference of ship-based and satellite-based radius (velocity) represented by triangles (circles). Blue (red) colors mark anticyclones (cyclones).

pothesis. Apart from that, all the values of V_{max} range between 40-80% without any correlation regarding sense of rotation or Rossby number. Nevertheless, V_{max} varies in a smaller range than R_{max} but without reaching estimates as good as R_{max}.
In conclusion, satellite-based estimations seem to be more accurate for large Rossby numbers. For smaller values of Ro, one can find good as well as inaccurate estimations of eddy parameters.

Proceeding to the second part of the comparison, features which were clearly visible in the surface vmADCP data but were not recognized by the gridded ADT map are investigated. There is one example during M160 which fits into this category: the Santiago eddy. The vmADCP measured velocities strongly refer to an existence of an eddy at the surface, but analyzing the ADT map from 26th of November 2019 no positive anomaly can be found, which would be assumed with strong surface velocities (Figure 11). It took until the 30th of November until an eddy could be discovered from satellite maps. Comparing the parameters from when the eddy manifested in the ADT maps, the AMEDA radius is 154% larger and the maximum azimuthal velocity is 65% smaller than the Gauss-Newton

estimate from the 26th of November. Still, a comparison between the two radii has to be done with caution as there is no proof that the velocity field is still the same as it was on the 26th of November. However, it is a strong feature which is assumed to gain strength since it developed a strong anomaly in the ADT maps, so it is very likely that it is still there on the 13th of December.

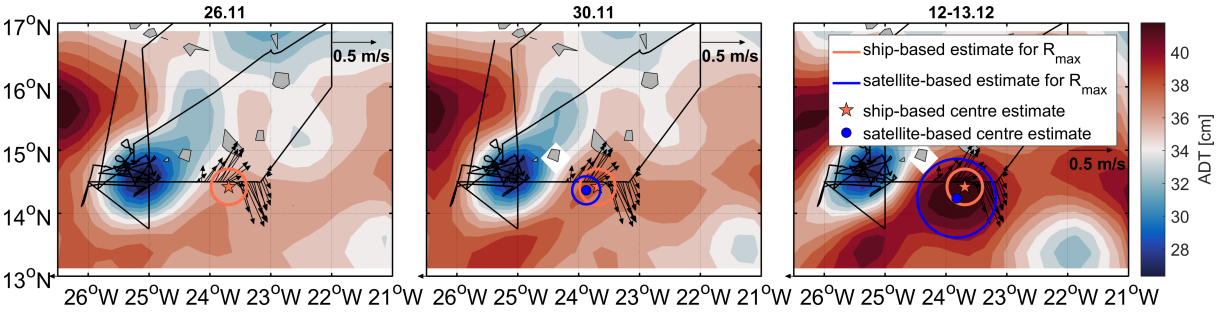

Figure 11: Santiago eddy on the 26th (left panel), 30th of November (middle) and 12-13th of December (right panel) on the ADT field, orange circles show ship based estimate from 26th of November, satellite-based estimates are displayed in blue, black arrows represent vmADCP section of the 26th of November.

The last part of the comparison focuses on features A1-A4 which are declared as eddies using satellite products, but which could not clearly be detected by the vmADCP data. There were several more eddies detected by the satellite-based method, but there were two restrictions that have to be made. Only eddies which are close to the ship track or even crossed by it and whose fit in the time period of the crossing can be further investigated. Otherwise, there would be no data to compare the satellite derived parameter to. During M156 there are no eddies which fit the criteria therefore this comparison focuses on M160.

It will be exemplified by the region northern of the islands close to Santo Nicolao and Sal. The satellite-based method detected a cyclone (A1) and an anticyclone (A2), which were touched by the ship track (Figure 12). Focusing on A1 (blue) first, the vmADCP shows only northward velocities during the whole crossing which do not correspond to the possible eddy estimation. The velocities at depth are weaker but show signs of an eddy-like structure with opposite velocity directions. But then those velocities would fit a cyclonic rotation rather than an anticyclonic. A2 (red) shows greater velocities in general. Due to its oval shape and that the ship track only leads along the rim an overall statement is difficult. However, one can see southward directed velocities at the western edge of the eddy which totally fit the cyclonic assumption. Those velocities are still visible at depth which strengthens the assumption of a possible feature.

Features A3 and A4 did not show any velocities in the vmADCP data that correspond to the satellite-based estimates (not shown).

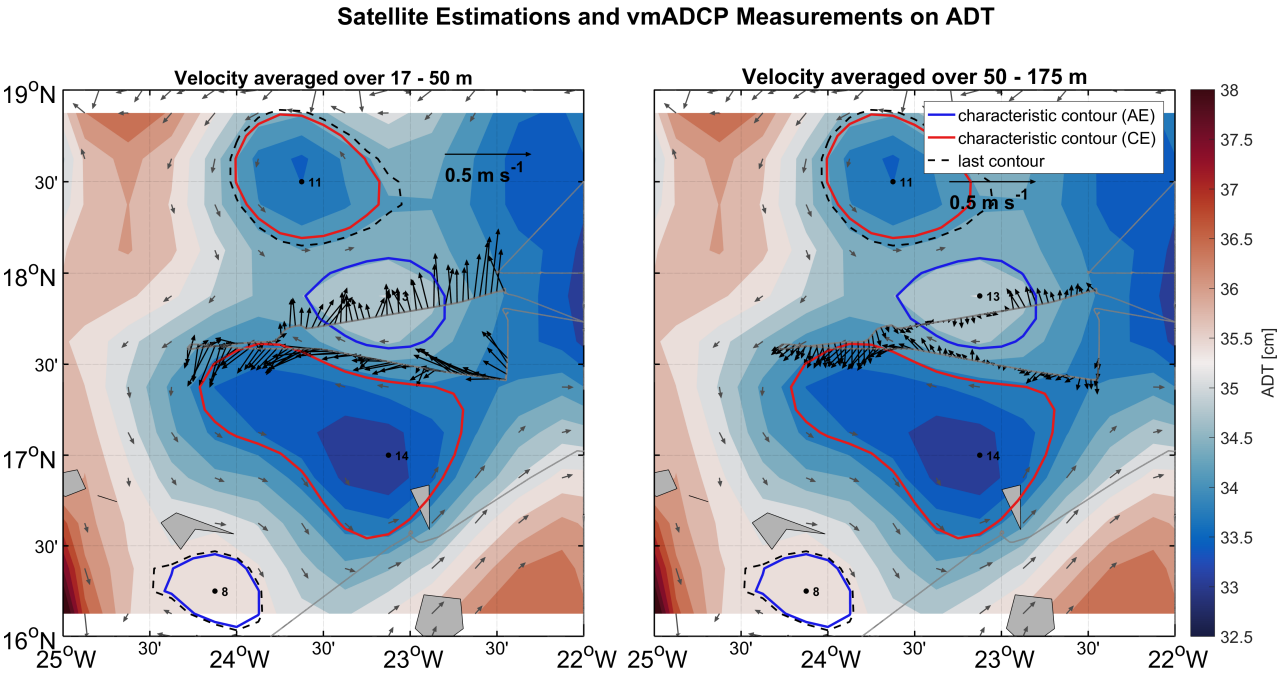

Figure 12: Features A1 and A2 with characteristic contours for cyclones (red) and anti-cyclones (blue) as well as the vmADCP sections along the ship track as black arrows and CMEMS-velocities as grey arrows. Velocities in the left panel are averaged over the upper 17-50m, in the right panel 50-175m are averaged.

Since satellite products give the opportunity to track eddies over time, one should consider investigating the evolution of the eddies as well to get a better understanding of reasons for the lack of detection in in-situ measurements.

A3 appeared on the ADT maps first on the 8th of December and was visible until the end of the cruise except for the 12th of December when it disappeared from the map for one day. That was the day after that region was crossed by the research vessel on the 11th of December. In the time between its appearance and the 12th of December the eddy radius changed size in a range between 24 and 32.5 km. One could observe same behavior for the velocity. After its reappearance it first lost size and speed but then enlarged and accelerated again until it reached values of about 43 km and 7 $^{cm}/_{s}$ for R_{max} and V_{max}, respectively. But nevertheless, several days before and after the survey the eddy showed a mean radius of 26 $\pm$ 5 km and a maximum azimuthal velocity of 4 $\pm$ 1 $^{cm}/_{s}$. The other features also showed a similar behavior. They often disappeared for some days from the satellite maps or changed their location.

4. Discussion

This study discussed the ability to detect eddies using altimetric data and compared it to the results based on ship measured velocities. The Angular Momentum Eddy Detection and Tracking Algorithm (AMEDA) tends to overestimate the radii by 68% in average and underestimates the maximum azimuthal velocity by also 44% compared to the nonlinear damping least-squares Gauss-Newton optimisation algorithm using vmADCP data. Nevertheless, some of the estimates are closer to ship-based estimates and others differ by much more than the mean.

Le Vu et al. (2018) tested AMEDAs sensitivity for eddy detection regarding the spatial grid resolution. Due to the coarse resolution of the global CMEMS products, their results were that AMEDA can not provide valid information for eddies with a radius smaller than $R_{max} \leq 2dX \approx 50$km where dX is the grid resolution. They showed that the eddy size will be overstated and the maximum velocity will be underestimated. This fits to the results of this study. The detected radii were mostly barely greater than 50 km or even smaller. The overall average of all detected eddies throughout the whole time period of the two cruises even turned out to be 44 km and therefore less than the recommended radius. This is consistent with Chelton et al. (2011b), who stated that the SSH fields can not adequately resolve the lower range of the radius scale of mesoscale variability ($\sim$40 km).

Other recent studies compared AMEDA to in-situ measurements and came to similar results. Ioannou et al. (2017) used data from drifters in the Mediterranean Sea as well as vmADCP data. They found that the estimations for the size were quite good but the maximum azimuthal velocity was underestimated by 45-60%. Garreau et al. (2018) also investigated eddies in the same region and found that the radius was overestimated by comparing it to lowered ADCP data and the rotational speed was underestimated by using drifter data as reference. Castelão and Johns (2011) used the Gauss-Newton method to characterize rings of the North Brazil Current and compared their results to Goni and Johns (2001) which used along-track altimetric data. Goni and Johns (2001) used a Gaussian model to describe the ring structure which only depends on the sea surface elevation and the radius of maximal azimuthal velocity. In addition, they used along track altimetry data. Castelão and Johns (2011) conclusion was that the eddies derived from satellite data were weaker but smaller than those from Goni and Johns (2001). Comparing the results they concluded that the Gaussian model can represent the sea surface height signature well but highly underestimates the intensity (V_{max}) of the eddies. This could be a result of the location of the satellite tracks. When they did not cross the centre of the eddy, the maximum elevation will be underestimated.

Moreover, Aroucha et al. (2020) used AMEDA to investigate North Brazil rings. Comparing their results to Castelão and Johns (2011), the radii estimated by AMEDA were 12% larger and the velocities underestimated by 70%. The Rossby number calculated by Castelão and Johns (2011) counted on average 0.33 while AMEDA determined 0.08 which would be 76% larger. Aroucha et al. (2020) used 24 years of data while Castelão and Johns (2011) analysed 10 eddies. Comparing those results to this study, the difference between the satellite and ship observed eddies was smaller while the difference of the estimated velocities was even higher. The Rossby numbers showed a similar difference between satellite-based and ship-based estimates.

Schütte et al. (2016) investigated eddies in the ETNA using 19 years of satellite products and found a mean radius of 56 ± 12 km which is 19 km or 51% larger than the mean ship-based radius detected in this study but closer to the mean satellite-detected radius.

Castelão and Johns (2011) found Rossby numbers ranging from 0.25-0.47 which indicates strong nonlinear features. Bendinger (2020) investigated eddies of two cruises in the Labrador Sea and found Rossby numbers ranging between 0.06 and 0.49 with an average of 0.17. In this study ship-based estimates of the Rossby number ranged between 0.13-0.33. Aroucha et al. (2020) determined the same mean Rossby number by using AMEDA like this study (0.08) which also lies in the same range of detected values by Chelton et al. (2011b). Using a satellite-based method they determined mostly values smaller than 0.1. So even if the Rossby number depends on latitude as well as on the specific properties of each eddy, satellite-based methods seem to determine significant smaller Rossby numbers than ship-based measurements. This is not surprising, since satellite-based eddy detection also tends to overestimate radii and underestimate velocities.

Searching for certain thresholds or indications to distinguish between good and inaccurate satellite-based estimates of eddy parameters, we found that large Rossby numbers can be an indicator for good satellite-estimates. Furthermore, eddies with velocities smaller than 0.06 and radii smaller than 40 km are likely to be a false detection. Radius and azimuthal velocity will be further discussed in the following along with four other possible thresholds or indicators including along-track data of SLA, sea surface temperature, the eddy's lifetime and its amplitude.

Since its coarse resolution, the global CMEMS data set suffers from smoothing and interpolating, the ability of representing the mesoscale eddy field is reduced (Amores et al., 2018). One future approach could be to use the satellite along track data in addition to the interpolated data set. This could be a chance to validate the smoothed and gridded data and see how the actual SLA may be different. This approach was performed on one

example. As mentioned prior the SLA data did not show a sign of the Santiago eddy. The CMEMS along track data set was used to plot fitting tracks for that region and on the day of the crossing (Figure 13). This elevation fits the ships observation where an anticyclonic eddy is associated with a positive SLA. This indicates that the smoothing and interpolating indeed can lead to biased SLA map, which in turn influences the SLA based eddy detection.

Consequently, along track data can help to validate the gridded maps. If the along track data show the same sea surface anomalies, the derived estimations may be more trustworthy.

However, it is a lucky coincidence that the satellite track crossed exactly through the centre of the eddy the day the vmADCP measurements were taken. Nonetheless, this example shows that analysing the along track SLA data can be helpful by validating the eddy detection through satellite products.

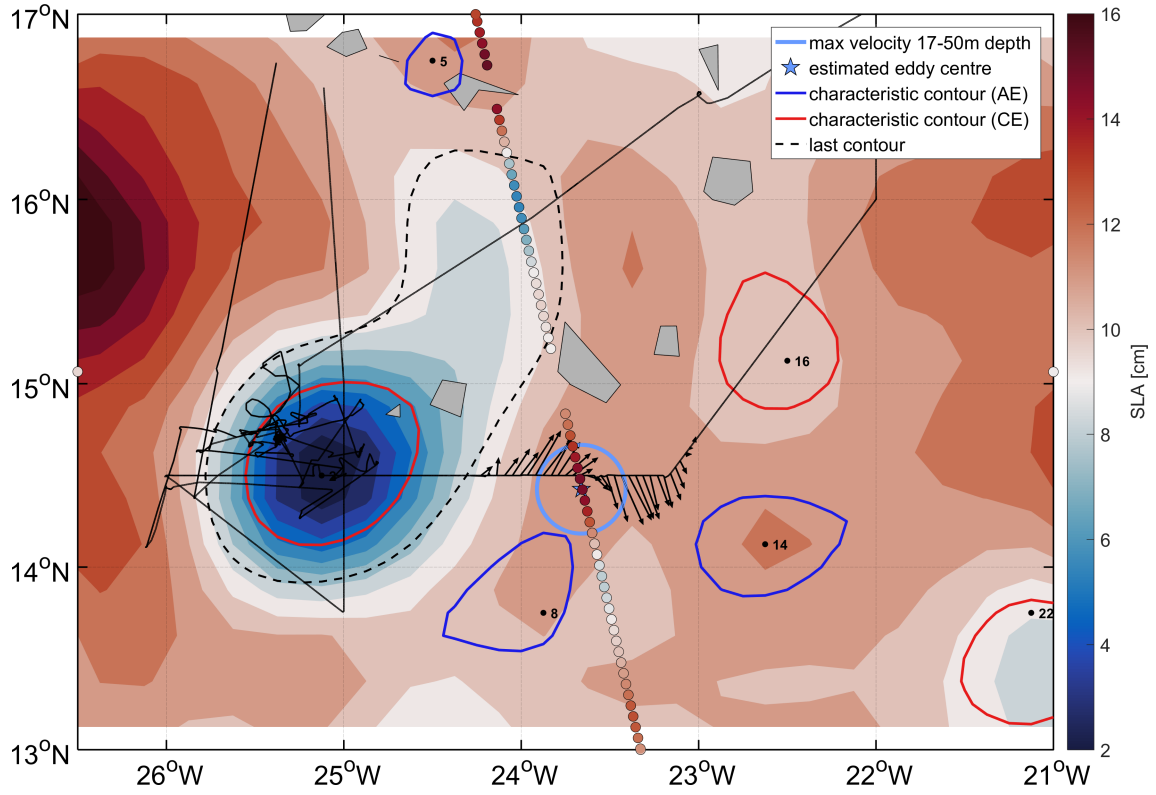

Figure 13: Santiago eddy estimate (light blue) on the 26th of November on SLA field with along-track SLA data. vmADCP data shown as black arrows, AMEDAs estimates in blue (anticyclone) and red (cyclone) with CMEMS-velocities in grey.

Other satellite products like sea surface salinity, chlorophyll or sea surface temperature could be used to validate the satellite-based eddy detection. Latter was further investigated in this study. Cyclones (anticyclones) are associated with a reduced (enhanced) sea

surface temperature (SST) (Schütte et al., 2016). The goal was to compare the SST field to the radii of the eddies and see how the SST corresponds to the horizontal scale of the eddy and if there are any parallels to the differences between the satellite and ship-based estimates. To validate the satellite derived SST it was compared to in-situ measurements along the ship track.

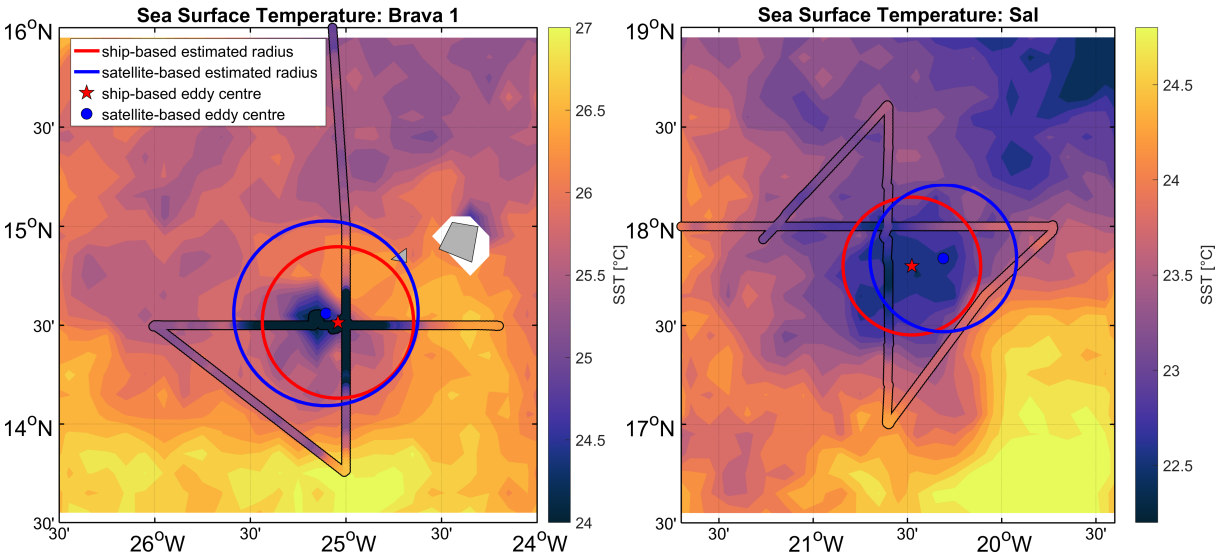

Figure 14: Satellite derived sea surface temperature (SST) and ship-measured SST along the cruise track with ship-based (red) and satellite-based (blue) estimates.

This approach was exemplified by three cyclonic eddies (Brava, Sal, E4). The radii of Sal and Brava were both well estimated by the satellite-based method. The sea surface temperature satellite maps confirm this estimation for Sal by showing a reduced temperature in about the same size as the estimated radius (Figure 14, right panel). Furthermore, the in-situ measurements agree with the satellite data. The satellite data show for the Brava eddy only a small negative temperature anomaly within the radius of the eddy (Figure 14, left panel). Comparing the satellite data to the ship measured sea surface temperature, it is noticeable that the reduced temperature stretches over a far larger area which fits to the estimated radius. Besides its inaccurate radius estimate, E4 does not show any reduced temperature neither in the satellite data nor in the in-situ measurements as well (Figure Appendix1).

During this investigation it became clear that the satellite data is highly restricted by cloud coverage. Therefore, one could consider to use satellite data which combine sensors based on infrared as well as on microwaves where latter are not limited by clouds. But then, the resolution of SST measured by microwaves (25 km) is not as good as the infrared-based (∼10 km) measurements.

In conclusion, a temperature anomaly which covers the whole area of the radius can be

an indication of an accurate eddy detection, but there are also good eddy estimations where the satellite SST data did not show a reduced radius-sized temperature field. If the temperature data did not show the suggested anomaly, this can be taken as an indication for an inaccurate estimate, but not necessarily for a false detection since E4 existed but not as big as the satellite data calculated. Further investigation regarding anticyclones and their correlation of SST and radius estimation needs to be done.

Another eddy characteristic one could use to qualify satellite estimations is the eddy's lifetime. Some studies used a minimum lifetime of 7 days as a threshold (Schütte et al., 2016; Amores et al., 2018). Analyzing the evolution over time of eddies A1-A4, it was shown that some of those features tend to be unstable by disappearing and reappearing on the satellite maps. Consquently, if an eddy is not changing size and strength over a certain period (like one week) it is more likely to be a real feature.

Chelton et al. (2011b) defined the amplitude of an eddy as the magnitude of the difference between the estimated height of the eddy boundary and the extremum value of SSH within the centre of the eddy. Then they used a minimum amplitude of 1 cm as a threshold for the eddy detection. Amplitudes of eddies were not investigated in this study but in future approaches such a threshold may be considered.

Schütte et al. (2016); Chelton et al. (2011b) defined thresholds regarding the radius of eddies. Schütte et al. (2016) only took eddies into account which were larger than 45 km, while Chelton et al. (2011b) stated that features smaller than 40 km can not be resolved. Suitable, the satellite-based estimates of this study showed a cut-off radius of 40 km. Features with smaller radii were likely to be false defections.

Last, one could use the maximum azimuthal velocity to define a threshold. Features detected by satellite products but not by in-situ measurements most of the time had maximum azimuthal velocities of lower than 7 $^{cm}/_{s}$, while velocities of well defined eddies reached values of more than 45 $^{cm}/_{s}$. But then the Sal eddy presents with a maximal azimuthal velocity of only 7 $^{cm}/_{s}$ as well. So even if this threshold may be true for most of the cases one should be careful not to miss real eddies as well.

Since the velocity measurements are taken by a acoustic doppler current profiler one should also take uncertainties regarding that instrument into account. The standard error of the mean velocity was assumed as 3 $^{cm}/_{s}$. Consequently, the uncertainties for small velocities are higher than for large ones. Therefore, the ability of the ADCP to display weak eddies like features A1-A4 can be questioned. Nevertheless, in most cases the ADCP data showed rather strong velocities which could not be associated with the satellite based estimates. Hence, that the ADCP due to its error missed those features

is rather unlikely. In addition, the ship-measured azimuthal velocities were significantly higher than the error of 3 $^{cm}/_{s}$ which makes it negligible small.

Summarizing the discussed possibilities to qualify satellite-based estimates, it was shown that along track data of sea surface height as well as satellite derived sea surface temperature may help to validate satellite-based estimates. Furthermore, one could introduce thresholds of minimum lifetime, radius, velocity or amplitude to role out false estimates. Further opportunities lie in additional data like sea surface salinity or chlorophyll.

As described above, eddies play a very important role in the global oceans and are subjects of interest in various research fields. To improve our understanding of the ocean system and the impact of eddies within that the first step is to identify and track eddies. The more precise our estimates are or the better we understand their weaknesses the better our results will be. A good estimate of size and location of the eddy is also important if one wants to do a in-situ survey.

From Le Vu et al. (2018) and Garreau et al. (2018) AMEDA seems to be a good tool to identify eddies and estimate the derived parameters if altimetric data with an fine grid resolution is available. Detecting and identifying eddies through satellite data still offers many advantages such as a global coverage in spatial and temporal resolution. It offers the opportunity to track eddies over a long period of time and over long distances without the need of in-situ measurements. However, the current altimetric products provided by CMEMS have a coarse resolution that would not allow AMEDA to provide valid information for small scale features. This study showed that AMEDA is able to find almost all eddies that were detected by vmADCP data, but could not picture the eddy in such a precise way. This could be done with the Gauss-Newton method.
In future studies Argo floats or similar data sets from gliders, saildrones, moorings or waveriders could be considered to broaden the data set. That could be an opportunity to receive more sections through an eddy which could provide parameters to emphasize the results.

In 2021 a new satellite mission Surface water and Ocean Topography (SWOT) will be launched which will provide data of the oceans surface in a much higher spatial resolution and will possibly allow to resolve the submesoscale. In addition, a global data set with a high resolution will allow a much better validation of the eddy field through satellite-based methods for eddy detection.

5. References

A. Amores, G. Jordà, T. Arsouze, and J. Le Sommer. Up to What Extent Can We Characterize Ocean Eddies Using Present-Day Gridded Altimetric Products? *Journal of Geophysical Research: Oceans*, 123(10):7220–7236, 2018. ISSN 21699291. doi: 10.1029/2018JC014140.

L. C. Aroucha, D. Veleda, F. S. Lopes, P. Tyaquiçã, N. Lefèvre, and M. Araujo. Intra- and Inter-annual variability of NBC rings using AMEDA algorithm: observations from 1993 to 2016. *Journal of Geophysical Research: Oceans*, pages 1–20, 2020. ISSN 2169-9275. doi: 10.1029/2019jc015921.

A. Bendinger. Characteristics of Mesoscale and Submesoscale Eddies in the Labrador Sea : Observations vs . Model. 2020.

G. P. Castelão and W. E. Johns. Sea surface structure of North Brazil Current rings derived from shipboard and moored acoustic Doppler current profiler observations. *Journal of Geophysical Research: Oceans*, 116(1):1–12, 2011. ISSN 21699291. doi: 10.1029/2010JC006575.

G. P. Castelão, L. C. Irber, and A. B. Villas Boas. An objective reference system for studying rings in the ocean. *Computers and Geosciences*, 61:43–49, 2013. ISSN 00983004. doi: 10.1016/j.cageo.2013.07.004. URL `http://dx.doi.org/10.1016/j.cageo.2013.07.004`.

A. Chaigneau, A. Gizolme, and C. Grados. Mesoscale eddies off Peru in altimeter records: Identification algorithms and eddy spatio-temporal patterns. *Progress in Oceanography*, 79(2-4):106–119, 2008. ISSN 00796611. doi: 10.1016/j.pocean.2008.10.013.

D. B. Chelton, R. A. Deszoeke, M. G. Schlax, K. El Naggar, and N. Siwertz. Geographical variability of the first baroclinic Rossby radius of deformation. *Journal of Physical Oceanography*, 28(3):433–460, 1998. ISSN 00223670. doi: 10.1175/1520-0485(1998)028⟨0433:GVOTFB⟩2.0.CO;2.

D. B. Chelton, J. C. Ries, B. J. Haines, L. L. Fu, and P. S. Callahan. Chapter 1 Satellite Altimetry. *International Geophysics*, 69(C):1–183, 2001. ISSN 00746142. doi: 10.1016/S0074-6142(01)80146-7.

D. B. Chelton, M. G. Schlax, R. M. Samelson, and R. A. de Szoeke. Global observations of large oceanic eddies. *Geophysical Research Letters*, 34(15):1–5, 2007. ISSN 00948276. doi: 10.1029/2007GL030812.

D. B. Chelton, P. Gaube, M. G. Schlax, J. J. Early, and R. M. Samelson. The influence

of nonlinear mesoscale eddies on near-surface oceanic chlorophyll. *Science*, 334(6054): 328–332, 2011a. ISSN 10959203. doi: 10.1126/science.1208897.

D. B. Chelton, M. G. Schlax, and R. M. Samelson. Global observations of nonlinear mesoscale eddies. *Progress in Oceanography*, 91(2):167–216, 2011b. ISSN 00796611. doi: 10.1016/j.pocean.2011.01.002. URL `http://dx.doi.org/10.1016/j.pocean.2011.01.002`.

A. M. Doglioli, B. Blanke, S. Speich, and G. Lapeyre. Tracking coherent structures in a regional ocean model with wavelet analysis: Application to Cape Basin eddies. *Journal of Geophysical Research: Oceans*, 112(5):1–12, 2007. ISSN 21699291. doi: 10.1029/2006JC003952.

J. H. Faghmous, I. Frenger, Y. Yao, R. Warmka, A. Lindell, and V. Kumar. A daily global mesoscale ocean eddy dataset from satellite altimetry. *Scientific Data*, 2:1–16, 2015. ISSN 20524463. doi: 10.1038/sdata.2015.28.

J. Fischer, P. Brandt, M. Dengler, M. Müller, and D. Symonds. Surveying the upper ocean with the ocean surveyor: A new phased array Doppler current profiler. *Journal of Atmospheric and Oceanic Technology*, 20(5):742–751, 2003. ISSN 07390572. doi: 10.1175/1520-0426(2003)20⟨742:STUOWT⟩2.0.CO;2.

T. Fischer. Diapycnal diffusivity and transport of matter in the open ocean estimated from underway acoustic profiling and microstructure profiling. 2011. URL `http://eprints.uni-kiel.de/12310/`.

I. Frenger, N. Gruber, R. Knutti, and M. Münnich. Imprint of Southern Ocean eddies on winds, clouds and rainfall. *Nature Geoscience*, 6(8):608–612, 2013. ISSN 17520894. doi: 10.1038/ngeo1863. URL `http://dx.doi.org/10.1038/ngeo1863`.

P. Garreau, F. Dumas, S. Louazel, A. Stegner, and B. Le Vu. High-Resolution Observations and Tracking of a Dual-Core Anticyclonic Eddy in the Algerian Basin. *Journal of Geophysical Research: Oceans*, 123(12):9320–9339, 2018. ISSN 21699291. doi: 10.1029/2017JC013667.

G. J. Goni and W. E. Johns. A census of North Brazil current rings observed from TOPEX/POSEIDON altimetry: 1992-1998. *Geophysical Research Letters*, 28(1):1–4, 2001. ISSN 00948276. doi: 10.1029/2000GL011717.

A. Ioannou, A. Stegner, B. Le Vu, I. Taupier-Letage, and S. Speich. Dynamical Evolution of Intense Ierapetra Eddies on a 22 Year Long Period. *Journal of Geophysical Research: Oceans*, 122(11):9276–9298, 2017. ISSN 21699291. doi: 10.1002/2017JC013158.

J. Isern-Fontanet, E. García-Ladona, and J. Font. Vortices of the Mediterranean Sea: An altimetric perspective. *Journal of Physical Oceanography*, 36(1):87–103, 2006. ISSN 00223670. doi: 10.1175/JPO2826.1.

Z. Lachkar and N. Gruber. A comparative study of biological production in eastern boundary upwelling systems using an artificial neural network. *Biogeosciences*, 9(1): 293–308, 2012. ISSN 17264170. doi: 10.5194/bg-9-293-2012.

B. Le Vu, A. Stegner, and T. Arsouze. Angular momentum eddy detection and tracking algorithm (AMEDA) and its application to coastal eddy formation. *Journal of Atmospheric and Oceanic Technology*, 35(4):739–762, 2018. ISSN 15200426. doi: 10.1175/JTECH-D-17-0010.1.

L. Marina. *Transport and Mixing in Geophysical Flows*. Number June. 2008. ISBN 9783540752158. doi: 10.1007/978-3-540-75215-8.

J. C. McWilliams. The vortices of two-dimensional turbulence. *Journal of Fluid Mechanics*, 219:361–385, 1990. ISSN 14697645. doi: 10.1017/S0022112090002981.

N. Mkhinini, A. L. S. Coimbra, A. Stegner, T. Arsouze, I. Taupier-Letage, and K. Béranger. Long-lived mesoscale eddies in the eastern Mediterranean Sea: Analysis of 20 years of AVISO geostrophic velocities. *Journal of Geophysical Research: Oceans*, 119(12):8603–8626, 2014. ISSN 21699291. doi: 10.1002/2014JC010176.

A. Okubo. Horizontal dispersion of floatable particles in the vicinity of velocity singularities such as convergences. *Deep-Sea Research and Oceanographic Abstracts*, 17(3): 445–454, 1970. ISSN 00117471. doi: 10.1016/0011-7471(70)90059-8.

D. Olson. Rings In The Ocean. *Annual Review of Earth and Planetary Sciences*, 19(1): 283–311, 1991. ISSN 00846597. doi: 10.1146/annurev.earth.19.1.283.

M.-I. Pujol, Y. Faugère, G. Taburet, S. Dupuy, C. Pelloquin, M. Ablain, and N. Picot. DUACS DT2014 : the new multi-mission altimeter dataset reprocessed over 20 years. *Ocean Science Discussions*, (January):1–48, 2016. ISSN 1812-0784. doi: 10.5194/os-2015-110.

F. Schütte, P. Brandt, and J. Karstensen. Occurrence and characteristics of mesoscale eddies in the tropical northeastern Atlantic Ocean. *Ocean Science*, 12(3):663–685, 2016. ISSN 18120792. doi: 10.5194/os-12-663-2016.

W. S. Von Arx and C. H. Dwight. An Introduction to Physical Oceanography. *American Journal of Physics*, 30(10):775–776, 1962. ISSN 0002-9505. doi: 10.1119/1.1941791.

J. Weiss. The dynamics of enstrophy transfer in two-dimensional hydrodynamics.

Physica D: Nonlinear Phenomena, 48(2-3):273–294, 1991. ISSN 01672789. doi: 10.1016/0167-2789(91)90088-Q.

6. Appendix

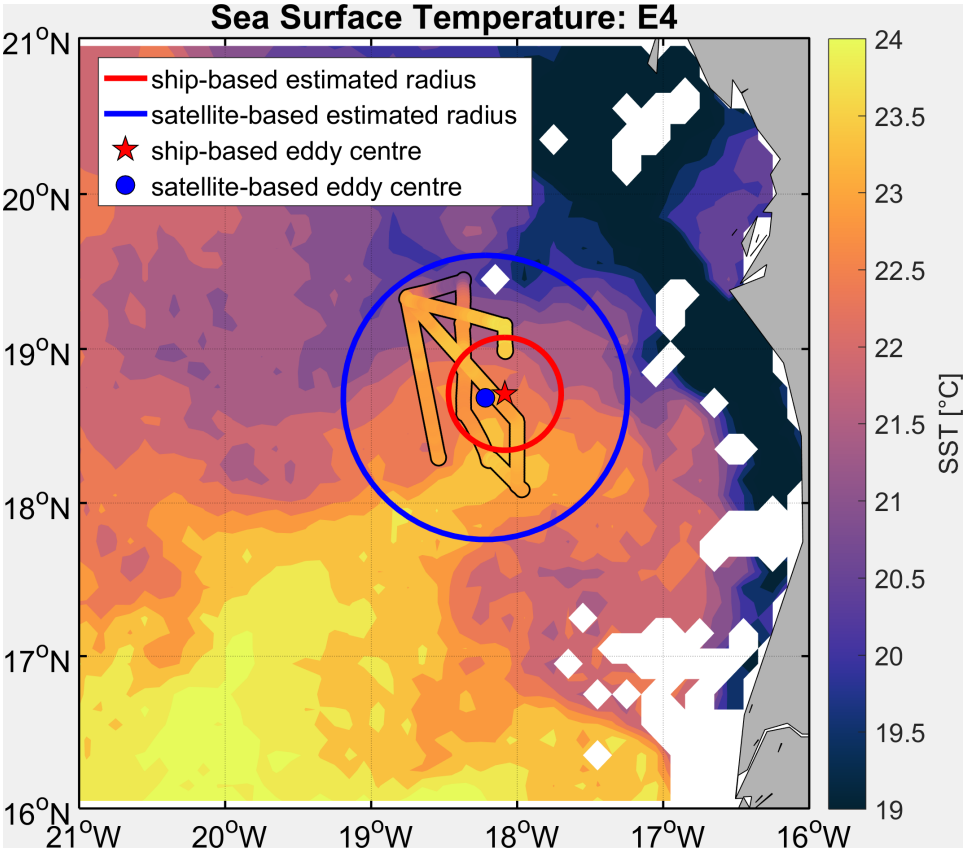

Figure Appendix1: Satellite derived sea surface temperature (SST) and ship-measured SST along the cruise track with ship-based (red) and satellite-based (blue) estimates.

Acknowledgements

I would like to thank Marcus Dengler for the opportunity, his guidance and support throughout this study. I also would like to thank Tim Fischer, Juri Knudsen and Johannes Karstensen for all the helpful discussions during the Wednesdays-meetings as well as Torge Martin.
Finally, I wish to thank my parents for their support during my studies.

Eidesstattliche Erklärung

Hiermit erkläre ich, dass ich die vorliegende Arbeit selbständig und ohne fremde Hilfe angefertigt und keine anderen als die angegebenen Quellen und Hilfsmittel verwendet habe. Die eingereichte schriftliche Fassung der Arbeit entspricht der auf dem elektronischen Speichermedium. Weiterhin versichere ich, dass diese Arbeit noch nicht als Abschlussarbeit an anderer Stelle vorgelegen hat.

Datum: 17.12.2020 Unterschrift: